Planetary and Space Science 117 (2015) 207–222

Contents lists available at ScienceDirect

Planetary and Space Science

journal homepage: www.elsevier.com/locate/pss

# On the status of orbital high-resolution repeat imaging of Mars for the observation of dynamic surface processes

P. Sidiropoulos *, J.-P. Muller

*Imaging Group, Mullard Space Science Laboratory/University College London, Holmbury St. Mary, Dorking, Surrey RH5 6NT, UK*

ARTICLE INFO

*Article history:*
Received 16 December 2014
Received in revised form
18 June 2015
Accepted 22 June 2015
Available online 3 July 2015

*Keywords:*
Mars
Orbital images
Mapping
Stereo
Metadata
Temporal analysis

ABSTRACT

This work deals with the meta-data analysis of high-resolution orbital imagery that was acquired over the last four decades of Mars. The objective of this analysis is to provide a starting point for planetary scientists who are interested in examining the martian surface in order to detect changes that are related to not fully understood natural phenomena. An image aggregation method is introduced and used to generate image groupings related to prioritising regions for change detection. The parameters determining each grouping are the season, the Martian Year and the local time that an image was acquired, the imaging instrument and its resolution. The analysis shows that there is sufficient coverage to systematically examine periodic martian phenomena in images that depict the same area over the same season, as well as sporadic martian phenomena (e.g. a new crater) in images that depict the same area in different time periods. The end product of this work is a series of 35 global coverage maps demonstrating the high-resolution repeat coverage of Mars up to Martian Year 31 under different temporal and viewing condition constraints. These are available both through supplementary material as well as via a web-GIS.[1]

© 2015 The Authors. Published by Elsevier Ltd. This is an open access article under the CC BY license (http://creativecommons.org/licenses/by/4.0/).

## 1. Introduction

The imaging of Mars through spacecraft technology started with the Mariner 4 flyby, which on 14 and 15 July 1965 acquired 21 low-resolution pictures that covered 1% of the martian surface.[2] Mariner 4 was followed 4 years later by the dual missions of Mariner 6 and 7, which acquired 201 images, covering some 20% of Mars with low resolution images.[3] Around the same time as the Soviet's Union Mars 2 and 3 spacecraft returned a total of 60 low-resolution images, the systematic imaging of Mars started with the Mariner 9 orbiter, which in 1971 and 1972 acquired 7329 images. Mariner 9 mapped nearly all the planet with resolution varying from 1 to 2 km/pixel and ≈2% of Mars with resolution reaching 100 m/pixel (NASA Scientific & Technical Information Office, 1974).

The limit of 100 m/pixel was exceeded by the Visual Image Subsystem on-board the twin spacecraft Viking Orbiter 1 & 2. The Viking Orbiters, launched in 1975, attained a global medium resolution coverage of Mars but also acquired images with resolution as fine as 8 m/pixel. After Viking Orbiter, four more orbiters, three from NASA and one from ESA, have been sent to Mars to image its surface with ever higher resolution imagery. The technology has improved significantly over the last decade, such that images with resolution as fine as 25 cm/pixel have been acquired with high image quality. This has allowed the identification of previously undiscovered dynamic surface phenomena and unusual surface features, as well as the examination of surface composition and geological history. A crucial role in this analysis is now being played by change detection modules, in which two images acquired at different times are compared in order to try to identify surface features that have changed in the meantime, irrespective of the lighting conditions but with little or no obscuration from clouds or dust. While change detection was originally tackled in a manual and non-systematic way, the increasing imaging rate with high resolution implies the need for a fully systematic approach that would maximise the exploitation of the available data.

The first step of such an approach would be to identify the martian regions that, based on the available data, should be prioritised for examination whether the surface appearance has changed. Even though this seems a rather straightforward goal, it does not have a unique solution. However, it can be approached differently depending on the main application objectives of the change detection task. For example, if change detection is performed so as to examine processes that happen periodically each and every martian season (e.g. seasonal flows at high latitude areas, McEwen et al., 2011), the prioritised regions should be the

* Corresponding author.
*E-mail addresses:* p.sidiropoulos@ucl.ac.uk (P. Sidiropoulos), j.muller@ucl.ac.uk (J.-P. Muller).

[1] www.i-Mars.eu
[2] http://nssdc.gsfc.nasa.gov/nmc/masterCatalog.do?sc=1964-077A
[3] http://nssdc.gsfc.nasa.gov/nmc/spacecraftDisplay.do?id=1969-014A

http://dx.doi.org/10.1016/j.pss.2015.06.017
0032-0633/© 2015 The Authors. Published by Elsevier Ltd. This is an open access article under the CC BY license (http://creativecommons.org/licenses/by/4.0/).

ones that show repeat coverage with high-resolution images taken during the same season. On the other hand, if change detection related to non-seasonal phenomena is performed, regions with multiple high-resolution coverage over several Martian Years should be prioritised.

In this work, we present several groupings of the available high-resolution Mars orbiter images, aiming to facilitate change detection in various application scenarios. Before presenting them, we should note that we use 2 thresholds to discriminate between high-resolution and medium-resolution images, namely 20 and 100 m/pixel, respectively. The first threshold is used when dealing with changes that can be observed only in very high-resolution images (such as spiders, Piqueux et al., 2003, and active gullies, Dundas et al., 2015), while the second threshold deals with changes that can be observed also in images with coarser resolution, such as slope streaks (Schorghofer et al., 2007) and dust devils (Verba et al., 2010). Of course there are changes observable only at the highest possible resolution (achieved for the time being only from HiRISE), such as Recurring Slope Lineae (RSL) (McEwen et al., 2014) and bedform migration (Bridges et al., 2013). However, the percentage of Mars that is covered more than once from HiRISE products is only 0.51%, thus making the systematic aggregation of these images unnecessary.

By default change detection involves temporal groupings (i.e. groupings according to the time that the image was acquired). The related analysis occupies a large part of this work. We conduct two temporal groupings of all of the high-resolution Mars imaging products (i.e. with a resolution finer than 100 m/pixel) that were acquired from orbiter missions from 22 June 1976 until 31st July 2013, i.e. the end of Martian Year 31 (according to the Clancy calendar, Clancy et al., 2000, for which the start of Martian Year 1 was 11 April 1955). The first grouping examines product distribution through Martian Years, so as to highlight those areas that favour the search for sporadic events, and the second analyses product distribution by season, to identify areas favouring the search for seasonally periodic events, such as phenomena related to seasonal frost at middle and high latitudes. Apart from the temporal groupings, high-resolution data are additionally grouped according to the image incidence angle, a parameter that determines the lighting conditions, thus being of major importance when looking for changes in features associated with the changing appearance of surface bi-directional reflectance. Finally, images are grouped based on the instrument that acquired them. This is conducted because most change detection to date is performed with pairs of images coming from a single instrument. The change detection potential of each camera is further outlined by an overlap analysis, which summarises the number of images that have mapped the same region of Mars with a set of overlapping thresholds.

All of the above groupings are presented through a series of tables, as well as repeat coverage maps, i.e. maps for which the colour scale corresponds to the number of times the martian surface was mapped. These are used to guide the ambitious work that is being conducted within EU FP7 i-Mars project, i.e. the orthorectification of all the available high-resolution Mars orbiter imagery and, subsequently, a global-scale automatic change detection processing. Note that all the maps that are presented here will be publicly available through a Web-GIS that is reachable on i-Mars website,[4] thus allowing for queries from scientists regarding the high-resolution coverage of Mars without having to duplicate the effort done for this work.

[4] http://www.i-mars.eu/web_gis

## 2. Mars orbiter exploration

The six orbiter missions, in chronological order, that conducted extensive high-resolution mapping of martian surface, are NASA's Viking Orbiter 1 (Soffen and Snyder, 1976), Viking Orbiter 2 (Soffen, 1976), Mars Global Surveyor (Albee et al., 2001), Mars Odyssey (Christensen et al., 2004), Mars Reconnaissance Orbiter (McEwen et al., 2007) and the ESA Mars Express (Neukum and Jaumann, 2004). As a result of the aforementioned 100 m threshold, pre-Viking Orbiter missions, such as Mariner 9, are omitted. India's Mars Orbiter Mission (MOM) is also omitted, since the temporal limit of this analysis is until the end of Martian Year 31, i.e. 31st July 2013, which is prior to launch of the mission.

The Viking Orbiter missions were the first to perform extensive high-resolution orbital mapping of the martian surface. Viking Orbiter 1 was launched on 20 August 1975 followed by Viking Orbiter 2, 20 days later (Soffen and Snyder, 1976). Both of them reached Mars at the beginning of the northern hemisphere summer of Mars Year 12 (Soffen, 1976) and performed global mapping during Martian Years 12–14 (i.e. between 1976 and 1980). The spatial resolutions varied significantly. Out of the approximately 47,000 orbiter images that were acquired by the Viking Orbiter missions, half were acquired with resolution between 100 m and 1 km/pixel, while the other half had resolution finer than 100 m, out of which approximately a thousand had resolution between 8 and 10 m/pixel. During the 4 years that Viking Orbiter acquired data, it achieved complete global coverage of Mars with resolution finer than 1 km/pixel and the first medium-resolution global mosaic of Mars (231 m/pixel at the equator).

After almost twenty years without an orbital presence at the planet (even though Phobos 2 acquired a little data during this interval), Mars Global Surveyor, with the Mars Orbiter Camera Narrow Angle (MOC-NA) and Mars Orbiter Camera Wide Angle (MOC-WA) on-board, reached Mars in September of 1997 (Albee et al., 2001), i.e. at the end of the northern hemisphere summer of Mars Year 23. The extensive imaging of the martian surface using these two cameras continued until 3 November 2006 (north hemisphere summer of Martian Year 28), during which 97,097 MOC-NA and 146,591 MOC-WA images were acquired (Malin et al., 2010). MOC-NA acquired images over selected regions of interest with a spatial resolution varying from 1.5 to 12 m/pixel. However, it should be noted that during aerobraking and science phasing orbits (phases that lasted from September 1997 until September 1998) MOC-NA was out of focus (Malin et al., 2010), thus producing images where most had neither scientific nor mapping value. Consequently, these images are omitted in the current work, leaving 95,966 images in total. Along with MOC-NA, MOC-WA repeatedly covered the planet with imagery of resolution that varied from 240 m to 7.5 km/pixel. Since the MOC-WA resolution range does not overlap with the one studied here, these MOC-WA images are also omitted from our analysis.

The next NASA orbiter to reach Mars having on-board cameras was the 2001 Mars Odyssey. Images are taken with the Thermal Emission Imaging System (THEMIS) (Christensen et al., 2004), which itself consists of the THEMIS-VIS camera for images in the visual reflected spectrum and the THEMIS-IR camera for thermal infrared emission spectrum images. Mars Odyssey entered orbit on 24 October 2001 (north hemisphere autumn of Martian Year 25) and is still fully working, therefore THEMIS is the longest surviving imager on-board an orbiter to date. Actually, the THEMIS-VIS nominal target was to map the 60% of the martian surface with a resolution of 18 m/pixel, but due to its longevity, it has surpassed this original target. It is noted that THEMIS-IR images are not taken into account both because their finest resolution is 100 m/pixel and because they are not visible spectrum (0.4–0.7 μm) images.

The only non-NASA orbiter mission up until the present-day that has also achieved near global mapping coverage of the martian surface is ESA's Mars Express (Neukum and Jaumann, 2004), with its High Resolution Stereo Coverage (HRSC) camera on-board (Jaumann et al., 2007; Scholten et al., 2005). Mars Express entered a highly elliptical orbit around Mars on 25 December 2003 (north hemisphere winter Martian Year 26) and continues imaging until today, achieving the most complete high-resolution multi-angle coverage so far, since HRSC is by default a stereo camera. The nominal HRSC resolution is 12.5–25 m/pixel for the nadir and most extreme off-nadir (18.9°) images respectively, a resolution that allows the generation of 3D models of the surface with spatial resolution 30–100 m (Gwinner et al., 2009). However, due to its elliptical orbit, the actual spatial resolution of each pixel depends on the current range distance from the martian surface. As a result, the spatial resolution may vary from 11 m to more than 100 m/pixel. Moreover, the mapping resolution may be different not only between orbits but also for surface regions that are mapped during a single orbit. In our analysis, we have selected to handle image footprints as elementary units and not to split them into sub-regions that have resolution within a given range. In order to reduce the errors caused by this choice, for each HRSC image the resolution at the start and at the end of the imaging is retrieved and their average is used to determine the resolution range that the image will be classified to. We have estimated that because 82% (94%) of HRSC images have a resolution less than 5 m (10 m) far from both the maximum and minimum image resolution, the average is appropriate to be used as the representative resolution value for the HRSC imagery. Finally, on-board Mars Express there is an imaging spectrometer OMEGA (IR Mineralogical Mapping Spectrometer), whose products are excluded in this work because OMEGA's resolution is 400–3000 m/pixel although OMEGA does cover the visible range.

The last orbiter mission under study is the NASA Mars Reconnaissance Orbiter, which was launched on 12 August 2005 and reached Mars on 10 March 2006 (north hemisphere spring of Martian Year 28). On-board are two high-resolution cameras, the High Resolution Imaging Science Experiment (HiRISE) (McEwen et al., 2007) and the Context Camera (CTX) (Malin et al., 2007). HiRISE acquires images at a local resolution (i.e. in selected regions of interest) of 0.25–0.5 m/pixel resolution, which is the best orbital imaging resolution that has been achieved so far. The high quality images acquired by HiRISE have revealed a number of hitherto unknown natural dynamic phenomena (e.g. McEwen et al., 2011; Chuang et al., 2010), thus reinforcing the need for a continuous high-resolution reconnaissance of the martian surface. On the other hand, CTX acquires images with 6 m/pixel resolution (and in less than 1% of the total CTX images, with 12 m/pixel) at a global scale. Due to its longevity, CTX has achieved the finest extensive coverage of the martian surface, imaging more than 82% of Mars. Both CTX and HiRISE instruments are still fully operating at the time of writing. On-board MRO there is also a Compact Reconnaissance Imaging Spectrometer for Mars (CRISM) (Murchie et al., 2007), whose products are excluded in this work since, even though they include visible wavelength data, they are not typically used as visible spectrum images.

## 3. Aggregating images for change detection

Change detection started with Viking Orbiter, when the extensive coverage of Mars with high-resolution images allowed the multi-temporal inspection of the most prominent martian features, such as the poles (Cutts et al., 1979). At the same time that change detection through the use of images acquired from a single instrument (mainly Viking Orbiter) was established, the first multi-instrument approaches were introduced, which used images from both Mariner 9 and Viking Orbiter missions to identify changes happening in specific regions-of-interest (e.g. to detect changes in the Cerberus region of Mars, Chaikin et al., 1981). However, single-instrument change detection is still a popular strategy, when dealing with change detection scenarios that require imagery with the finest available resolution (i.e. MOC-NA before 2006, Piqueux et al., 2003, and HiRISE after 2006, Thomas et al., 2010; Bridges et al., 2013; McEwen et al., 2014; Hansen et al., 2015). For example, in Bridges et al. (2013) HiRISE pairs are used to examine bedform migration because the speed that this phenomenon happens may be less than 10 cm/year, while in McEwen et al. (2014) RSL are found to be in almost all cases detectable only in HiRISE products.

On the other hand, there are a number of change detection techniques that are mainly based on pairs of single-instrument images, but also use images coming from other instruments in a secondary role. An important example of such a use can be found in new impact crater detection. The originally proposed method in Malin et al. (2006) suggested the use of MOC-WA images to detect seemingly dark blobs, which are formed over a large area (up to 1000 times larger than the actual crater size, Daubar et al., 2013) around the new crater from excavated material; subsequently, if pairs of MOC-NA images, acquired before and after the candidate impact, were available, they were compared to decide whether a new impact crater could be declared, otherwise (as happened in most cases, due to the limited MOC-NA repeat coverage) a new impact was declared if a fresh-appearing crater at the centre of the blast pattern was found. This approach was updated in Daubar et al. (2013), by replacing MOC-WA with CTX images and MOC-NA with HiRISE images. Moreover, it is noted that after a crater is identified all available images are inspected to temporally constrain the impact. The sub-set of craters that exposed ground ice were further examined in Dundas et al. (2014) without referring to any additional imaging products. Finally, Dundas et al. (2015) aimed at monitoring active gullies using pairs of HiRISE images, even though pairs of CTX images were used to first spot candidate active gully instances.

Change detection analyses in which multi-instrument pairs are straightforwardly compared were common after Mars Global Surveyor reached Mars, offering a chance to observe the evolution of surface features over the time period after Viking Orbiter. Confined by the fine resolution that a number of surface changes require to be detected and the sparse high-resolution coverage of Viking Orbiter, comparisons focussed on the most common changes in Mars, such as albedo changes and slope streaks. More specifically, in Fenton et al. (2007) a global analysis of the Mars albedo changes was conducted, by comparing Viking IRTM to MGS TES products. Global albedo changes were also the target for Geissler (2005), in this case using MOC-WA and Viking VIS images. On the other hand, slope streak formation and evolution were the topic in Aharonson et al. (2003) and Schorghofer et al. (2007), in both cases using MOC-NA to MOC-NA as well as MOC-NA to Viking pairwise comparisons. In recent work, the straightforward use of multi-instrument pairs is either avoided or applied only to studies dealing with local regions-of-interest, in which the available single-instrument pairwise data is limited. For example, in Verba et al. (2010) the dust devils in Gusev and Russell craters are studied through HiRISE, CTX and MOC-NA imaging products.

As far as we know, the only systematic approach to date, aiming to aggregate multi-instrument high-resolution data on a global scale, was conducted in a slope streak analysis work (Schorghofer and King, 2011). The authors implemented a graph representing the relative positions of available high-resolution Mars orbital images, before exploring the set of pairwise overlapping images for surface modifications related to slope streaks.

However, in Schorghofer and King (2011) each image footprint is determined exclusively by its four corners, which are assumed to be connected by straight lines. This assumption is valid near the equator (where slope streaks mostly appear) but if it is generally applied to Mars it would lead to severe artefacts near the poles. Moreover, the created graph does not include any georeference information about the overlapping images, which are given as lists of overlapping products. As a matter of fact, these lists were subsequently manually parsed to discard those acquired at latitudes that slope streaks are not expected. Finally, after prioritising regions with repeat coverage they used single-instrument pairs to actually identify the slope streak changes in a small number of sites.

On the contrary, we suggest that pairwise multi-instrument change detection should not be generally avoided, except when dealing with types of change that imply resolution achieved by a single instrument. The multi-instrument aggregation that is therefore introduced satisfies this principle at a global scale, thus additionally contributing an overall assessment of the martian surface imaging coverage. The aggregation output includes georeference information, in order to allow geolocated queries, as well as the placement of the output in a web-based GIS.

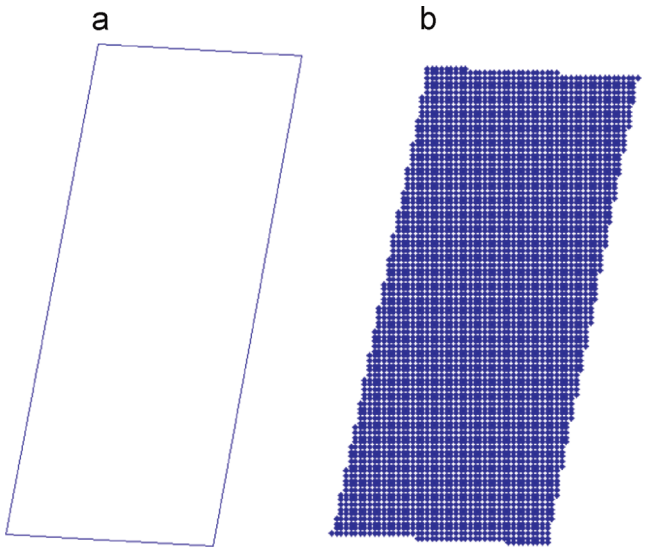


**Fig. 1.** (a) Footprint perimeter of THEMIS-VIS image V07794005RDR. (b) Quantised footprint area of THEMIS-VIS image V07794005RDR estimated by a raster region filling algorithm.

## 4. Materials and methods

### 4.1. Quantising image footprints

The crux of our aggregation system is about estimating and quantising the area that was mapped by an image, using as an input its footprint projected onto the planetary surface. The latter are available from the Mars Orbital Data Explorer (ODE) website (http://ode.rsl.wustl.edu/mars/indextools.aspx?displaypage=footprint), which is part of the NASA Planetary Data System (PDS) geosciences node. Actually, footprints are meta-data files including information about the time that the image was acquired, the orbiter position and orientation at that time, the camera characteristics (spatial resolution, focal length, etc.), the latitude and longitude range of the imaged martian surface, etc. The perimeter of the imaged area is represented through a series of consecutive linear segments, which are given as endpoints in a latitude–longitude coordinate system.

In order to quantise the footprint area that is determined by its perimeter a latitude-longitude raster of Mars is defined with constant sampling rate, $s$. Subsequently, the footprint area is estimated by a raster region filling algorithm (Henrich, 1994) (Fig. 1). Note that the binning step, $s$, in our implementation is 0.01°, which at the martian equator is equal to 600 m, thus is fine enough for the global statistical analysis that we are conducting. A smaller quantisation step is not expected to significantly enhance the accuracy, since for almost all martian orbiter images, the mapped surface (i.e. the footprint size) is much larger than the selected quantisation step. For example, HiRISE's and MOC-NA's swath width, the shortest among the included cameras, are 6 km and 3 km, respectively (McEwen et al., 2007; Malin et al., 2010). Moreover, by performing coregistration of NASA products to HRSC Orthorectified Images (ORIs) and Digital Terrain Models (DTMs) we have found that the latitude–longitude values provided from http://ode.rsl.wustl.edu/mars/indextools.aspx?displaypage=footprint often diverge from the actual mapped location by an offset that may reach up to several hundred metres. Consequently, the maximum achievable spatial accuracy is by default on the order of hundreds of metres, i.e. within the currently selected $s$ value.

### 4.2. Repeat coverage and overlap analysis

The mapping approach developed is summarised in Fig. 2. More specifically, for any valid combination of parameters (comprised the resolution, the camera name, the time that the image was acquired, the incidence angle and a stereo coverage flag), a repeat coverage matrix $M$ is defined (initially, $M(i, j) = 0$ for all $i$ and $j$). Subsequently, each martian orbital image $I$ satisfying the above parameters is quantised according to the analysis of Section 4.1 and the resulting raster is used to update $M$, which at the end of this process shows the number of times each (binned) point in the martian surface has been mapped (by images satisfying the selected parameters).

The resulting grid is transformed to a map using a Mollweide projection (Snyder, 1987), while for images of latitude higher than 60° a polar stereographic projection (Snyder, 1987) is additionally employed. Both Mollweide and polar stereographic projections are equal-area projections (i.e. martian surface regions with equal area are mapped to image regions with equal area) (Snyder, 1987), consequently, these maps can be straightforwardly used to extract global statistics for the high-resolution coverage of Mars.

In the current work, the following coverage analysis studies were conducted:

1. *Global coverage*: the overall coverage that was achieved from all instruments before the end of Martian Year 31. As already said, the vernal equinox of 11 April 1955 is adopted as the beginning of Mars Year 1 (MY1) (Clancy et al., 2000), thus placing 1st January 2015 at the end of autumn of MY32 and Viking Orbiter launch at MY11.
2. *Single-instrument coverage*: the coverage of Mars with high-resolution images that was achieved by each of the cameras sent before the end of Martian Year 31. Exceptionally, Viking Orbiter 1 and 2 products are considered to derive from the same instrument.
3. *Single-instrument stereo coverage*: the stereo coverage of the martian surface that was achieved by pairs of images from the same instrument. Also in this case, Viking Orbiter 1 and 2 products are considered to derive from the same instrument. In instruments such as HRSC, the instrument configuration is enough to detect stereo pairs. In all other cases, we have

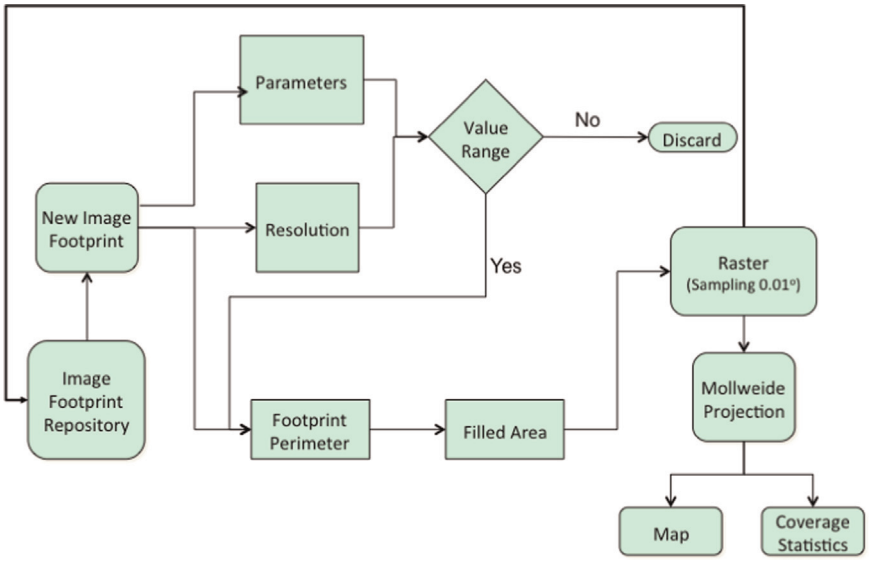


**Fig. 2.** A flowchart of the method developed to calculate coverage statistics of all Mars orbital imagery.

employed the criteria used to identify CTX stereo pairs,[5] i.e. the incidence angle of both images being less than 89°, the incidence angle difference less than 10°, the sub-solar azimuth difference less than 45° and the slew angle larger than 8°.

4. *Single-instrument overlap rate:* For each instrument (exceptionally, Viking Orbiter 1 and 2 VIS cameras are considered as a single instrument) an estimate of the number of images that overlap with $N$ more images of the instrument, when the overlap threshold is selected 1%, 5%, 20%, 50% and 75%. For this analysis the pipeline is modified so as to accept two image footprints as an input, estimating their overlap (instead of raster updating) after area filling.
5. *Seasonal coverage*: the coverage of Mars achieved at (north hemisphere) spring, summer, autumn and winter.
6. The coverage of Mars achieved between MY12-14, MY23-25, MY26-28 and MY29-31. In this work we refer to this type of coverage also as "epoch" coverage.
7. *Incidence angle coverage*: the coverage of Mars achieved with incidence angle 0–15°, 15–30°, 30–45°, 45–60°, 60–75° and 75–90°.

Additionally, the reader should note that the resolution of the visible spectrum cameras that image the surface of Mars varies from 25 cm/pixel for HiRISE to thousands of metres per pixel for Viking Orbiter. In order to impose some structure to our analysis and focus on dynamic surface phenomena, all images with resolution coarser than 100 m/pixel are here ignored. The rest of the images is grouped into two classes, the former consisting of images with resolution finer than 20 m/pixel (including all MOC-NA images, CTX and HiRISE images and a sub-set of THEMIS-VIS, HRSC, Viking Orbiter 1 and Viking Orbiter 2 images) and the latter consisting of images with a resolution of 20–100 m/pixel (including most Viking Orbiter 1 and 2 images and a sub-set of HRSC and THEMIS-VIS images). Note that only for HRSC products, due to the elliptical orbit of Mars Express, the resolution may significantly vary for pixels of the same image, thus only HRSC images are classified according to their mean resolution from the start until the end of the image for the nadir panchromatic camera only. For all other products, the resolution refers to the centre of the image projected onto the martian surface.

Finally, the reader is reminded that a martian day (i.e. a "sol") lasts 24 h, 39 min and 35 s and a Martian Year has approximately 668.6 sols or 686 (Earth) days, 23 h and 31 min (Allison, 2008). Due to the elliptical orbit of Mars around the sun, the seasons of Mars are not of equal duration. The length of the northern hemisphere spring, summer, autumn and winter is 193.3, 178.64, 142.7 and 153.95 sols, respectively (or 198.62, 183.55, 146.62 and 158.18 earth days) (Allison, 2008). In order to be able to deal with this, it is common to count martian time using areocentric longitude, $L_s$, which is the relative seasonal advance of the sun, counted in degrees. $L_s$ ranges from 0° to 359°, while a value equal to 0°, 90°, 180° and 270° correspond to the Mars northern hemisphere vernal equinox, summer solstice, autumnal equinox, and winter solstice, respectively (Allison, 2008).

## 5. Coverage analysis results

### 5.1. Method validation

Before starting the statistical analysis, the accuracy of the method was assessed. To do this, we compared global camera statistics extracted with our technique against the official results reported by the corresponding mission team. More specifically, 5 coverage statistics that are available for 3 high-resolution cameras were employed:

1. The MOC-NA final coverage of Mars that is reported in the mission overview published in Malin et al. (2010). The reported value (including out-of-focus products of the first mission phase) of the surface of Mars that was mapped at least once was 5.45%, while our estimate is 5.42% (5.27% when the first phase products are omitted).
2. The surface of Mars that was mapped at least once and more than once until April 2013 from CTX, which is given in Bell et al. (2013). The values reported by the mission team in Bell et al. (2013) are 82.2% and 34.6%. Our respective estimates are 82.07% and 34.52%.
3. The unique coverage that HRSC achieved with resolution finer

[5] https://raw.githubusercontent.com/zmoratto/Mars3DGearman/master/CTX_stereo_pair.txt

**Table 1**
Repeat martian surface coverage with resolution finer than 20 m/pixel, between 20 m/pixel and 100 m/pixel and finer than 100 m/pixel.

| Repeat coverage | Resolution < 20 m (%) | 20 m < Resolution < 100 m (%) | Resolution < 100 m (%) |
|---|---|---|---|
| Not covered | 3.24 | 11.5 | 0.15 |
| Once | 12.07 | 21.94 | 1.49 |
| Twice | 23.31 | 23.36 | 5.79 |
| Thrice | 22.98 | 17.35 | 12.05 |
| Four times | 16.78 | 10.31 | 16.58 |
| Five or six times | 14.45 | 8.76 | 31.12 |
| Seven–nine times | 4.64 | 3.35 | 21.48 |
| More than ten times | 2.53 | 3.43 | 11.34 |

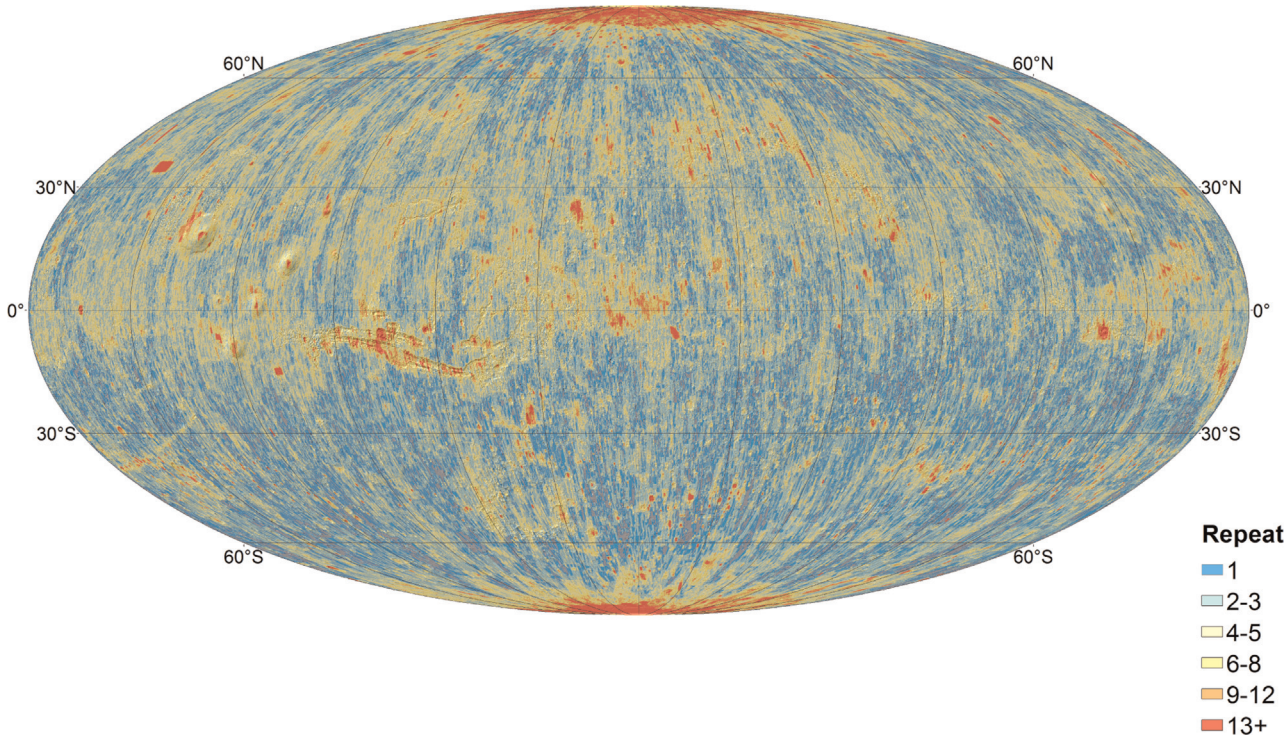


**Fig. 3.** The overall repeat coverage of Mars with resolution finer than 20 m/pixel.

than 20 m and finer than 100 m/pixel until 19 November 2013, are given in Hoffmann and the HRSC Experiment Team (2014), i.e. 67.2% and 96.5%, respectively. Our corresponding estimates until July 2013 are 66.28% and 96.14%.

From the 5 sets of comparison values, only the HRSC <20 m estimate differs from the actual value more than 1% in relative values (0.92% in absolute values or 1.37% in relative values). Consequently, it can be assumed that the estimated values have an accuracy, which is satisfactory for the analysis that is subsequently conducted.

### 5.2. Global Mars coverage

Initially, the different sources are ignored and instead, a histogram of the repeat image coverage of the martian surface is estimated (Table 1). Two distinct resolution thresholds are used, 20 m and 100 m/pixel. Table 1 implies that the median coverage of the martian surface is 6 images with resolution finer than 100 m and 4 images with resolution finer than 20 m/pixel. Moreover, 38.62% of the martian surface has been mapped less than 3 times with resolution finer than 20 m/pixel, a value that falls to 7.43% if we include images with resolution between 20 and 100 m/pixel. These statistics demonstrate that it appears to be generally feasible to perform an extensive comparison of the different images corresponding to the same area. Maps showing the overall coverage with resolution finer than 20 m, between 20–100 m and finer than 100 m is shown in Figs. 3, 4 and 5, respectively.

### 5.3. Single-instrument coverage

The coverage that each camera has achieved can be found in Table 2. This Table demonstrates that the orbiter cameras can be classified into two categories, the former aiming at imaging specific martian surface regions with very high-resolution (MOC-NA, HiRISE) while the latter is aimed at imaging the entire surface of Mars, at the expense of resolution (THEMIS-VIS, HRSC, CTX). From these three cameras, HRSC has achieved the most complete mapping of the martian surface with resolution finer than 100 m/pixel while CTX has the most complete mapping with resolution finer than 20 m/pixel. Furthermore, the longevity of THEMIS-VIS results in 82.01% coverage, thus providing an additional source of global Mars imagery. Overall, the above statistics demonstrate that for a large part of Mars, at least 3 different imaging sources can be found with resolutions finer than 100 m/pixel. MOC-NA and HiRISE provide additional sources for regions of increased scientific interest, while Viking Orbiter allows the analysis of the temporal evolution of approximately 23% of the martian surface for the last 20 Martian Years. Fig. 6 shows a plot of the surface coverage that each high-

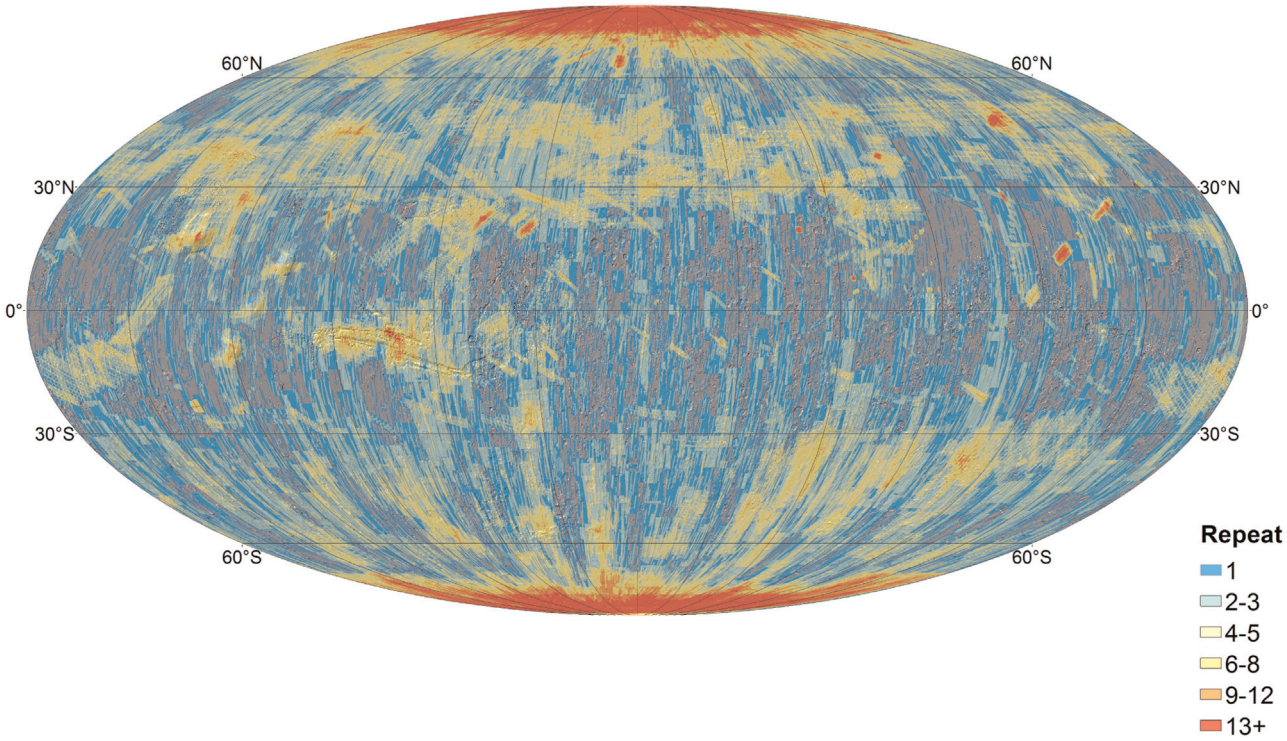


**Fig. 4.** The overall repeat coverage of Mars with resolution 20–100 m/pixel.

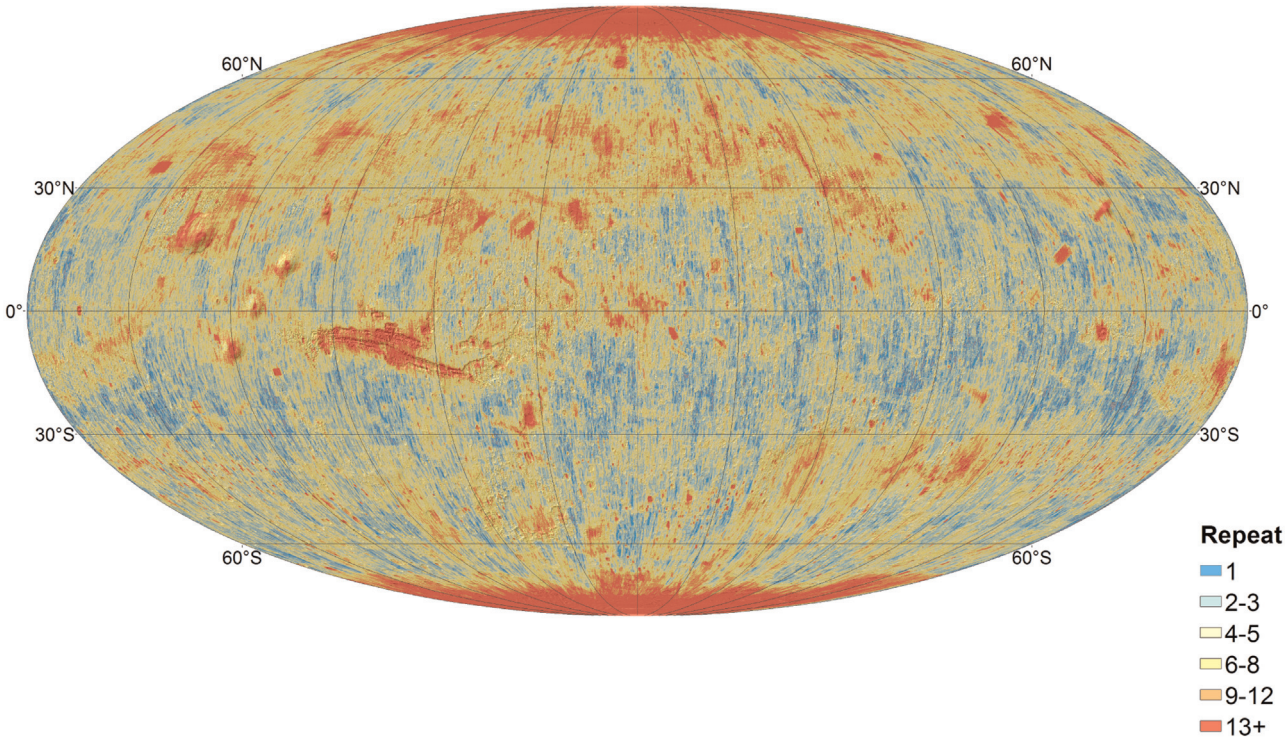


**Fig. 5.** The overall repeat coverage of Mars with resolution finer than 100 m/pixel.

resolution orbiter camera has achieved as a function of the resolution. For each resolution finer than 100 m/pixel, a line parallel to the *x*-axis is drawn, with length corresponding to the unique coverage that the instrument has achieved.

### 5.4. Single-instrument stereo coverage

There is a lot of work still to be done towards the completion of high-resolution global 3-D models of Mars. Moreover, HRSC is the

only camera with single-pass stereo mapping capabilities. HRSC images are used to generate DTMs with a resolution of 50–100 m/pixel (Gwinner et al., 2009). These can be subsequently bundle block adjusted, thus generating continuous 3-D models of large areas of Mars. However, according to the HRSC team, only 42.31% of Mars has been processed to the date of writing, but there are plans to generate a global 3-D high-resolution model of Mars within the iMars project (van Gasselt, 2015).

The achieved stereo and DTM coverage is shown in Table 3. This table implies that stereo coverage beyond HRSC is rather sparse, even for the cameras that have achieved substantial imaging of large parts of the martian surface. As a matter of fact, THEMIS-VIS products are by default nadir images, consequently they do not have any stereo capabilities, while stereo coverage achieved from CTX is only 2.79%. The apparent discrepancy associated with CTX repeat coverage (which is 34.78%) with the CTX stereo coverage is demonstrated in Figs. 7 and 8. Finally, MOC-NA and HiRISE stereo coverage is only 0.32% and 0.21%. Currently the HiRISE team has processed and released stereo products covering only 0.02% of the surface area of Mars. The above statistics demonstrate that the global stereo mapping of Mars with the set of currently available products would require the development of robust stereo techniques that successfully combine images with differences in the point spread function, the resolution, the season that were acquired, etc., which is not a trivial task (Thornhill et al., 1993; Kirk et al., 2002).

**Table 2**
High-resolution camera coverage. "Cov." stands for coverage, i.e. the martian surface that was imaged from each camera with a resolution between 0.25 and 20 m/pixel and 0.25 and 100 m/pixel, respectively. "Rep. Cov" stands for repeat coverage, i.e. the martian surface that was mapped more than once from each camera with a resolution between 0.25 and 20 m/pixel and 0.25 and 100 m/pixel, respectively.

| Camera | Cov. (20 m) (%) | Cov. (100 m) (%) | Rep. Cov. (20 m)(%) | Rep. Cov. (100 m)(%) |
|---|---|---|---|---|
| HiRISE | 1.4 | 1.4 | 0.5 | 0.5 |
| CTX | 82.71 | 82.71 | 34.78 | 34.78 |
| HRSC | 64.39 | 96.14 | 20.69 | 68.73 |
| THEMIS-VIS | 61.08 | 82.01 | 23.06 | 48.53 |
| MOC-NA | 5.27 | 5.27 | 0.54 | 0.54 |
| Viking Orbiter 1 & 2 | 0.56 | 22.69 | 0.12 | 12.2 |

### 5.5. Single-instrument overlap rate

In this analysis, we examine the overlap extent demonstrated by the products of the martian high-resolution orbital cameras, in order to assess their potential to be used for single-instrument change detection. The overlap ratio $R_{mn}$ of a pair of images $I_m$ and $I_n$ is defined as:

$$R_{mn} = \frac{|I_m \cap I_n|}{|I_m|} \quad (1)$$

where operator $|.|$ represents the area of an image and operator $\cap$ the common area (i.e., the intersection) of two images. We consider two images to be overlapping when $R_{mn} > T$, where $T$ is an overlap threshold. In this work 5 overlap thresholds are employed, 1%, 5%, 20%, 50% and 75%.

For an instrument, $C$, and a threshold, $T$, the overlap function $V_{C,T}(m)$ assigns to each image, $I_m$, the number of images acquired by instrument, $C$, for which $R_{mn} > T$. Finally, the mean value of $V_{C,T}(m)$ is estimated in order to extract the overlap rate of Table 4. Since for a small fraction of images (corresponding to images acquired over regions-of-interest such as the poles and the candidate landing sites) $V_{C,T}(m)$ is very large, biasing the estimated average value, we discard as outliers all $V_{C,T}(m)$ that are outside the $[\mu - 2\sigma, \mu + 2\sigma]$ range, where $\mu$ and $\sigma$ are the mean and the standard deviation of $V_{C,T}(m)$ and then estimate the average of the remaining $V_{C,T}(m)$ values as the actual overlap rate. Note that in this analysis the images taken into account for each instrument (i.e. being included in $C$) are those with resolution finer than 100 m/pixel. Moreover, for each image $I_m$ of an instrument $C$ we estimated the maximum overlap $R_{mn}$ that is achieved when $I_n$ parse the set of images belonging to $C$ ($I_n$ also satisfy the

**Table 3**
Stereo and publicly available DTM coverage for each camera.

| Camera | Stereo coverage (Res. <20 m/pixel) (%) | DTM coverage (Res. <100 m/pixel) (%) |
|---|---|---|
| HiRISE | 0.21 | 0.02 |
| CTX | 2.79 | 0 |
| HRSC | 64.39 | 42.21 |
| THEMIS-VIS | 0 | 0 |
| MOC-NA | 0.32 | 0 |
| Viking Orbiter 1 & 2 | 0.23 | 0 |

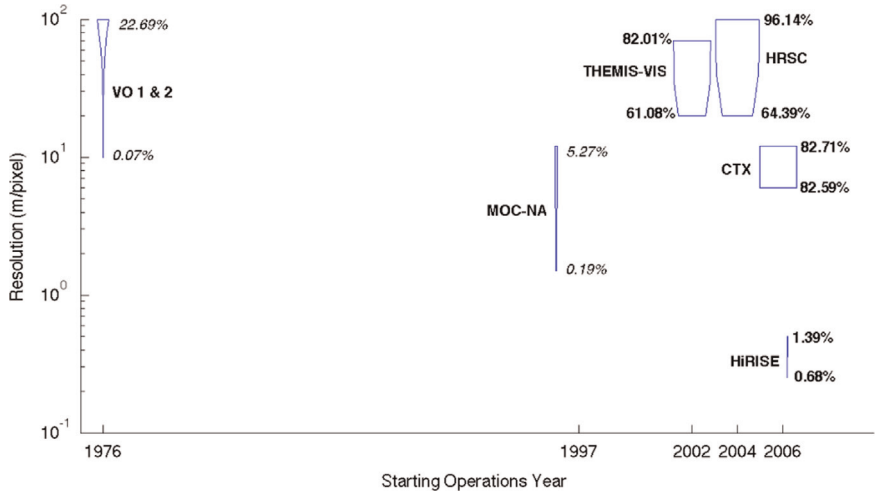


**Fig. 6.** The surface (unique) coverage of each high-resolution orbiter camera as a function of the resolution. The coverage of instruments that are no longer operating is shown in italics.

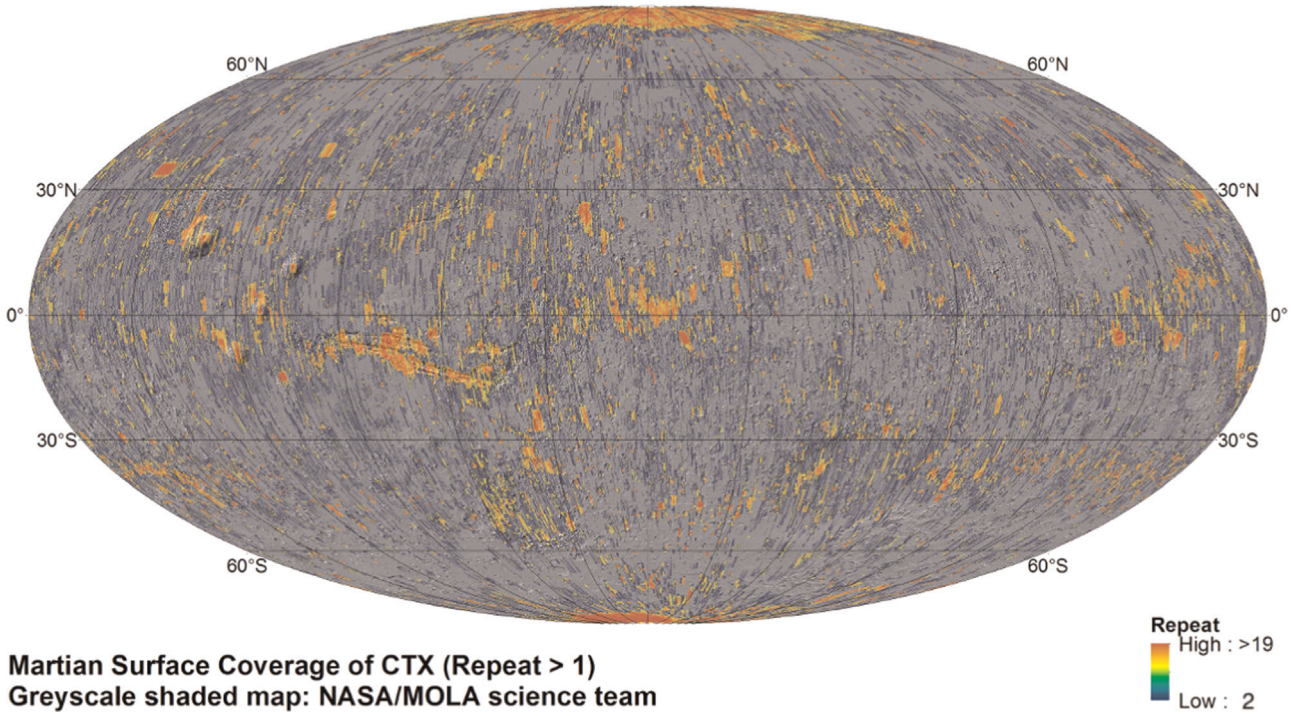


**Fig. 7.** Mars surface that was imaged by multiple CTX images including stereo.

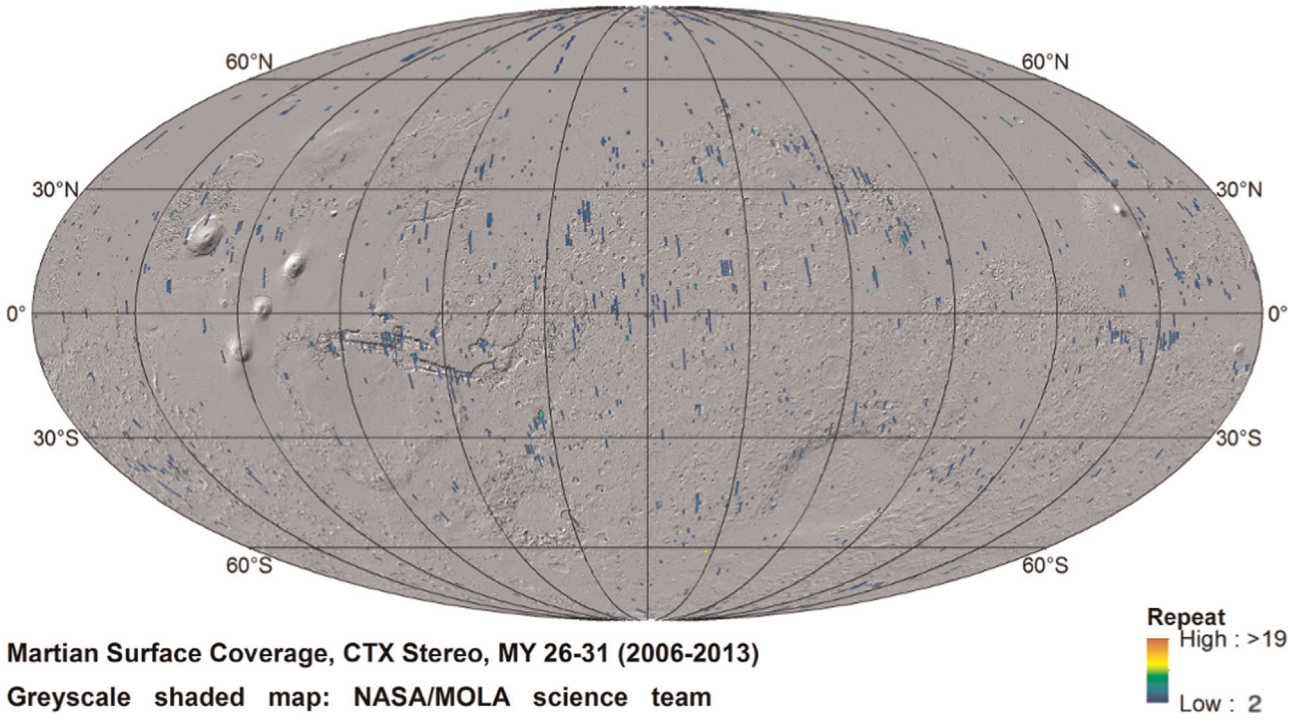


**Fig. 8.** Mars surface that was imaged by CTX images that form stereo pairs.

**Table 4**
Single-instrument overlap rate using overlap thresholds 1%, 5%, 20%, 50% and 75%.

| Camera | $T=1\%$ | $T=5\%$ | $T=20\%$ | $T=50\%$ | $T=75\%$ |
|---|---|---|---|---|---|
| HiRISE | 1.052 | 0.985 | 0.953 | 0.434 | 0.387 |
| CTX | 6.962 | 4.898 | 2.501 | 1.663 | 1.27 |
| HRSC | 9.933 | 6.841 | 3.864 | 1.523 | 0.789 |
| THEMIS-VIS | 6.978 | 5.582 | 2.712 | 1.218 | 0.409 |
| MOC-NA | 0.878 | 0.803 | 0.302 | 0.179 | 0.105 |
| Viking Orbiter 1 & 2 | 6.29 | 5.34 | 2.282 | 0.848 | 0.248 |

aforementioned resolution constraint). A histogram of the maximum overlap values for each instrument is shown in Fig. 9.

Both Table 4 and Fig. 9 support the use of multi-instrument pairwise comparisons for surface change detection. As a matter of fact, Fig. 9 show that more than 50% of HiRISE images and more than 60% of MOC-NA images would become useless if change detection is restricted only to single-instrument pairs. On the other hand, HiRISE and MOC-NA images are typically acquired in Mars regions-of-interest, in which changes are more probable to be found. Thus, when examining changes that can be detected in

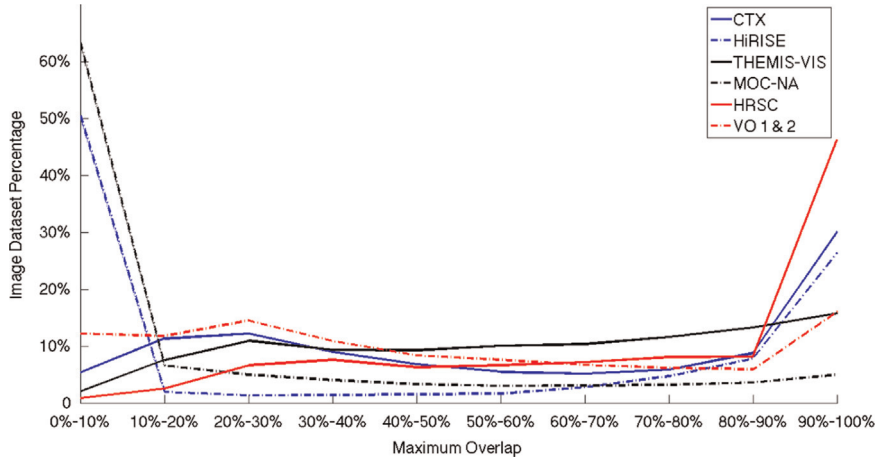


**Fig. 9.** Histogram of the maximum single-instrument overlap.

**Table 5**
Martian surface repeat coverage statistics according to the (Martian) season. Outside (inside) parentheses values correspond to the 100 (20) m/pixel statistics.

| NH Season | Spring | Summer | Autumn | Winter |
|---|---|---|---|---|
| Not covered | 16.85% (33.59%) | 31.96% (52.21%) | 34.78% (61.84%) | 39.6% (50.98%) |
| *Repeat* ≥ 1 | 83.15% (66.41%) | 68.04% (47.79%) | 65.22% (38.16%) | 60.4% (49.02%) |
| *Repeat* ≥ 2 | 57.11% (33.3%) | 36.95% (17.49%) | 32.27% (13.01%) | 28.81% (18.42%) |
| *Repeat* ≥ 3 | 32.91% (13.9%) | 18.77% (6.14%) | 14.17% (4.27%) | 13.02% (6.8%) |
| *Repeat* ≥ 4 | 17.08% (5.39%) | 9.72% (2.63%) | 6.42% (1.62%) | 6.48% (2.82%) |
| *Repeat* ≥ 5 | 8.85% (2.2%) | 5.45% (1.46%) | 3.31% (0.76%) | 3.82% (1.38%) |

images with the resolution of CTX, HRSC and THEMIS-VIS, the inclusion of HiRISE and MOC-NA images into multi-instrument pairs would increase significantly the number of identified changes. Additionally, even when examining the instruments that have achieved global coverage, if substantial overlap is required (e.g. 50%) the expected number of overlapping single-instrument images is no more than 2 (Table 4). On the contrary, the reader is reminded that in Section 5.2 we estimated that the median repeat coverage with images of resolution finer than 100 m/pixel is 6. Consequently, when searching overlapping images to compare with a high-resolution image, a median value of 5 multi-instrument images would be available, from which at most only 2 is expected to be from the same instrument.

### 5.6. Seasonal coverage

Table 5 shows the statistics of the high-resolution coverage during different martian seasons. A first conclusion that can be drawn is that the coverage depends on but is not determined by the season duration. As a matter of fact, northern hemisphere spring which is the longest season, demonstrates substantially larger coverage than any other season, including summer which is only 10% smaller than spring. On the other hand, summer's and winter's small coverage could be partially explained by the fact that, just like on Earth, the southern (northern) latitude zones of Mars are mostly in the dark during the North hemisphere summer (North hemisphere winter). Since we are dealing with images in the visual spectrum, this feature determines a pattern in which images are acquired according to the season. Consistent with the season-dependent image acquisition is the high-resolution coverage percentage of both summer and winter, which is almost equal and close to 50% (47.79% and 49.02%, respectively). The sparse autumn coverage, that reaches merely 38.16% of the surface for images with resolution finer than 20 m/pixel, is a side-effect of the increased dust activity during this season over the southern hemisphere (Smith, 2009) as well as the varying data rate from spacecraft to Earth, according to the Earth-Mars distance (Zurek and Smrekar, 2007). Actually, the last four oppositions (during which the data rate is maximised) happened on North hemisphere spring and summer, thus during MRO, Mars Odyssey and Mars Express missions the high data-rate period is disproportionally represented in these seasons.

Overall, Table 5 implies that there is adequate repeat coverage for the same season, since 13.01–33.3% of the martian surface was mapped more than once with resolution finer than 20 m/pixel, while 13.02–32.91% is covered from at least three images with resolution finer than 100 m/pixel. Thus, it becomes apparent that a substantial area of Mars can be examined to analyse the characteristics of currently unknown periodic phenomena, based on any distinct and common features in images of the corresponding area taken during the same season. Figs. 10 and 11 show the coverage of Mars with imaging products of resolution finer than 20 m/pixel for northern hemisphere spring and autumn, respectively. Additionally, Fig. 12 shows the polar region coverage during northern hemisphere spring. In this case, polar stereographic projection is used instead of Mollweide projection that is preferred for global coverage maps.

### 5.7. Epoch coverage

Table 6 refers to the martian surface that was covered during the four examined MY periods (referred to in this work also as "epochs"), i.e. MY 12-14 (starting 19 December 1975 and ending 9 August 1981), MY 23-25 (starting 27 August 1996 and ending 18 April 2002), MY 26-28 (starting 19 April 2002 and ending 8 December 2007), and MY 29-31 (starting 9 December 2007 and ending 31 July 2013). This table shows that near-global high-resolution Mars coverage has been independently achieved in two different time periods, in MY26-28 and MY29-31. Between Martian Years 26 and 28 only 60% of the surface was mapped with resolution finer than 20 m/pixel, thus global coverage requires the inclusion of images with coarser resolution. On the contrary, between Martian Years 29 and 31 almost 90% of the martian surface is covered exclusively by images with resolution finer than 20 m/pixel (Fig. 13).

The recent high-resolution mapping intensification becomes apparent from the fact that the Mars surface mapped more than once with resolution finer than 20 m/pixel at MY 29-31 (61.93%) was larger than the overall surface mapped with the same

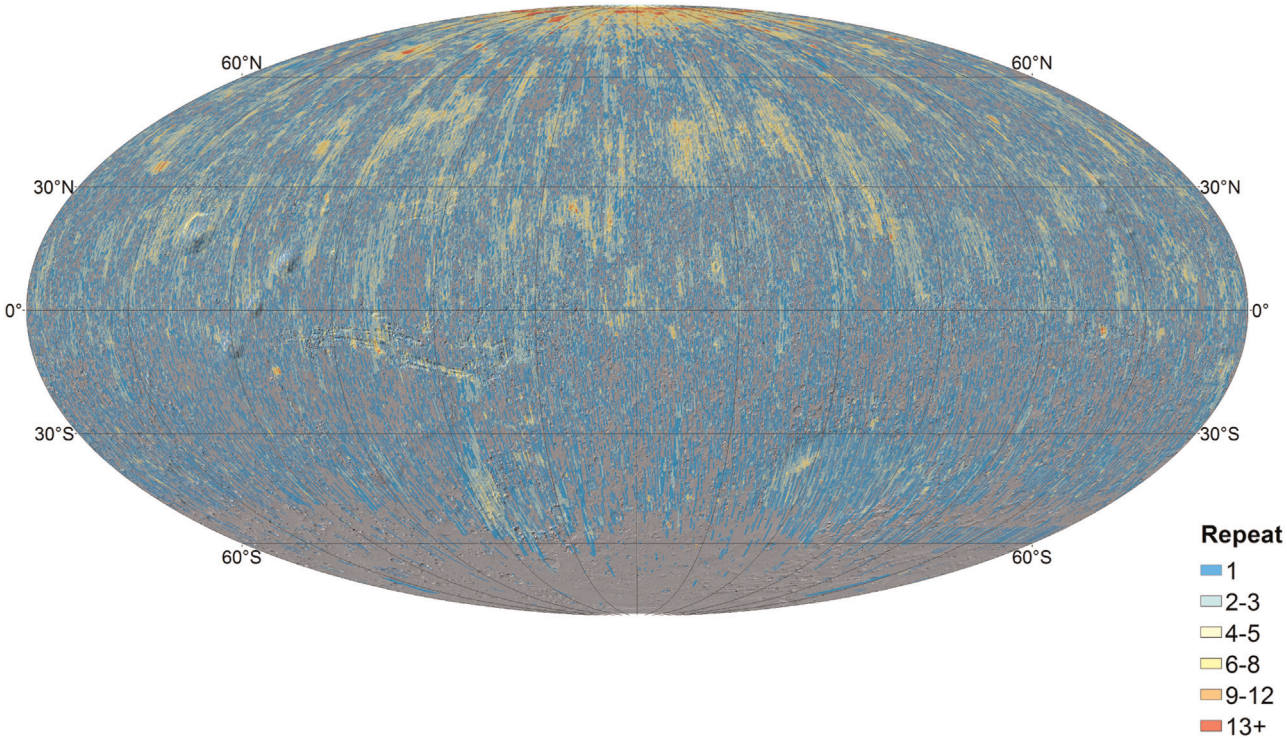


**Fig. 10.** The overall coverage of Mars with resolution finer than 20 m/pixel during North Hemisphere spring ($0° < L_s < 90°$).

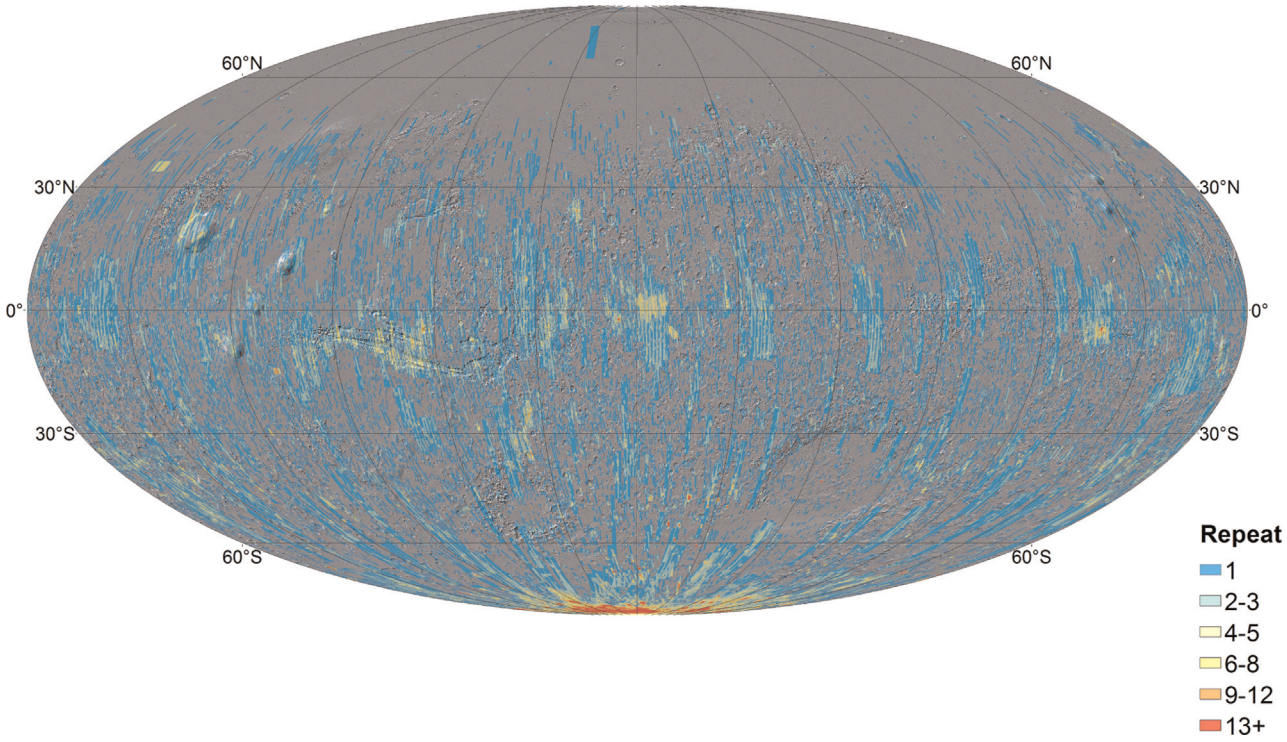


**Fig. 11.** The overall coverage of Mars with resolution finer than 20 m/pixel during North Hemisphere autumn ($180° < L_s < 270°$).

resolution at MY26-28 (59.93%). However, in both time periods an extensive part of Mars was repeatedly imaged with high-resolution, thus the (non-periodic) dynamic analysis of martian phenomena can be straightforwardly conducted for the last (earth) decade. On the contrary, before MY26 there is only a sparse mapping of Mars with high resolution (3.16% in MY23-25 and 0.56% in MY12-14). At the same time, a significant percentage of the martian surface was mapped with resolution 20–100 m/pixel (3.18% in MY23-25 and 22.69% in MY12-14), which implies that a successful merging of products with different resolutions would be essential in order to employ older data.

We additionally examined the mapping spread in the employed set of epochs, in order to discriminate between regions that were mapped repeatedly during different epochs and those that were

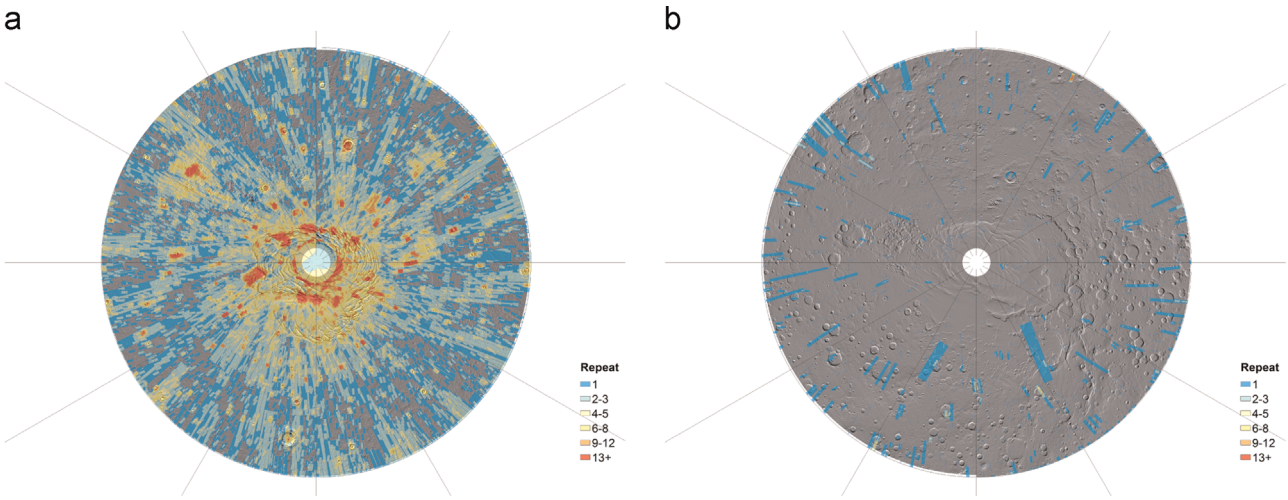


**Fig. 12.** (a) The overall coverage of the North pole of Mars with resolution finer than 20 m/pixel during North Hemisphere spring ($0° < L_s < 90°$). (b) The overall coverage of the South Pole of Mars with resolution finer than 20 m/pixel during North Hemisphere spring ($0° < L_s < 90°$).

**Table 6**
Martian surface repeat coverage statistics according to the (Martian) time period. Outside (inside) parentheses values correspond to the 100 (20) m/pixel statistics, respectively.

| MY Period | MY12-14 | MY23-25 | MY26-28 | MY29-31 |
|---|---|---|---|---|
| Not covered | 77.31% (99.44%) | 96.82% (96.84%) | 11.85% (40.07%) | 5.25% (11.47%) |
| *Repeat* ≥ 1 | 22.69% (0.56%) | 3.18% (3.16%) | 88.15% (59.93%) | 94.75% (88.53%) |
| *Repeat* ≥ 2 | 12.2% (0.12%) | 0.25% (0.25%) | 65.57% (29.53%) | 79.2% (61.93%) |
| *Repeat* ≥ 3 | 5.42% (0.04%) | 0.05% (0.05%) | 41.57% (13.18%) | 54.93% (34.54%) |
| *Repeat* ≥ 4 | 2.54% (0.01%) | 0.02% (0.02%) | 24.19% (5.94%) | 31.77% (16.7%) |
| *Repeat* ≥ 5 | 1.32% (0%) | 0.01% (0.01%) | 13.95% (2.85%) | 16.42% (7.84%) |

mapped extensively but during a single epoch (e.g. because they were candidate rover landing sites). For this analysis, we clustered the surface of Mars into 9 categories:

- Areas never mapped, which form class A.
- Areas mapped once, which form class B.
- Areas mapped twice or more, all times at the same epoch. These form class C.
- Areas mapped twice, but at two different epochs (D).
- Areas mapped at least three times but, at just two epochs (E).
- Areas mapped thrice, once time for three different epochs (F).
- Areas mapped at least four times, at three different epochs (G).
- Areas mapped once for each of the epochs (H).
- Areas mapped at least five times, at all four of the epochs (I).

The statistical analysis for images of resolution finer than 20 m/pixel and 100 m/pixel can be found in Table 7. This table shows that almost half of the martian surface has been mapped more than three times, in two distinct epochs. Having said that, the two resolution ranges exhibit different spread characteristics. More specifically, if only the images with the finest resolution are taken into account then 45.02% of Mars has been mapped in one epoch, while only 3.32% of Mars has been mapped during three or more epochs. On the contrary, if images with resolution between 20 and 100 m/pixel resolution are also included in the analysis, the surface percentage that has single-epoch coverage falls to 24.5% and the surface that has been mapped at least in three different epochs increase to 19.3%. These statistics imply that any global long-term studies of Mars surface changes, using the currently available datasets, is required to include images of lower resolution. This means that certain features on Mars cannot be studied for these time periods as they do not appear in these lower resolution images. The multi-epoch coverage of Mars for images with resolution finer than 20 m/pixel is shown in Fig. 14.

Finally, we estimated the timespan $T$ between the first and the last image, when both of them have resolution finer than a threshold. The threshold set for this estimation was {1, 3, 5, 7, 10, 30, 50 and 100} m/pixel. For each resolution threshold two kinds of statistics were estimated, a 6-bin temporal histogram (the percentage of $T$ that is less than 1 MY, 1-2 MY, 2-3 MY, 3-5 MY, 5-10MY and more than 10 MY) and the theoretical maximum Area-Time Factor (ATF) (Daubar et al., 2013). It is reminded that ATF was defined in Daubar et al. (2013) for crater counting as an equivalent to the area in which the size-frequency distribution of craters is scaled, in the case when the area is not uniformly covered by images acquired at the same time. Actually, ATF is estimated by dividing the input area into elementary patches, before the timespan $T$ between the first and the last image of the patch is estimated and multiplied by the patch size. The sum of all the elementary ATFs gives the overall ATF. Since the largest area over which crater counting can take place is the whole martian surface, we could use $T$ to estimate for each resolution threshold its theoretical maximum ATF (TMATF). Both the temporal histogram and the TMATF are given in Table 8.

### 5.8. Incidence angle coverage

The appearance of numerous surface features depends on the illumination conditions, which can be modelled to a great extent from the incidence angle when employing, for example, a Lambertian approximation of the martian surface bidirectional reflectance distribution function (BRDF). Incidence angle is defined at the centre of the image, as the angle $\theta$ between the sun's position and a vector perpendicular to the surface. Actually, incidence angle is a seasonally-independent measure of the local time, since values between 0° and 90° correspond to daytime, while values between 90° and 180° are night-time. More specifically, during the morning, the incidence angle decreases from 90° to a minimum value (depending on the season and the latitude), which is reached at noon. Afterwards, the incidence angle start to increase, exceeding 90° when the sun falls below the horizon at sunset.

The examined instruments do not have the capability of imaging during the night, thus the incidence angle of all high-

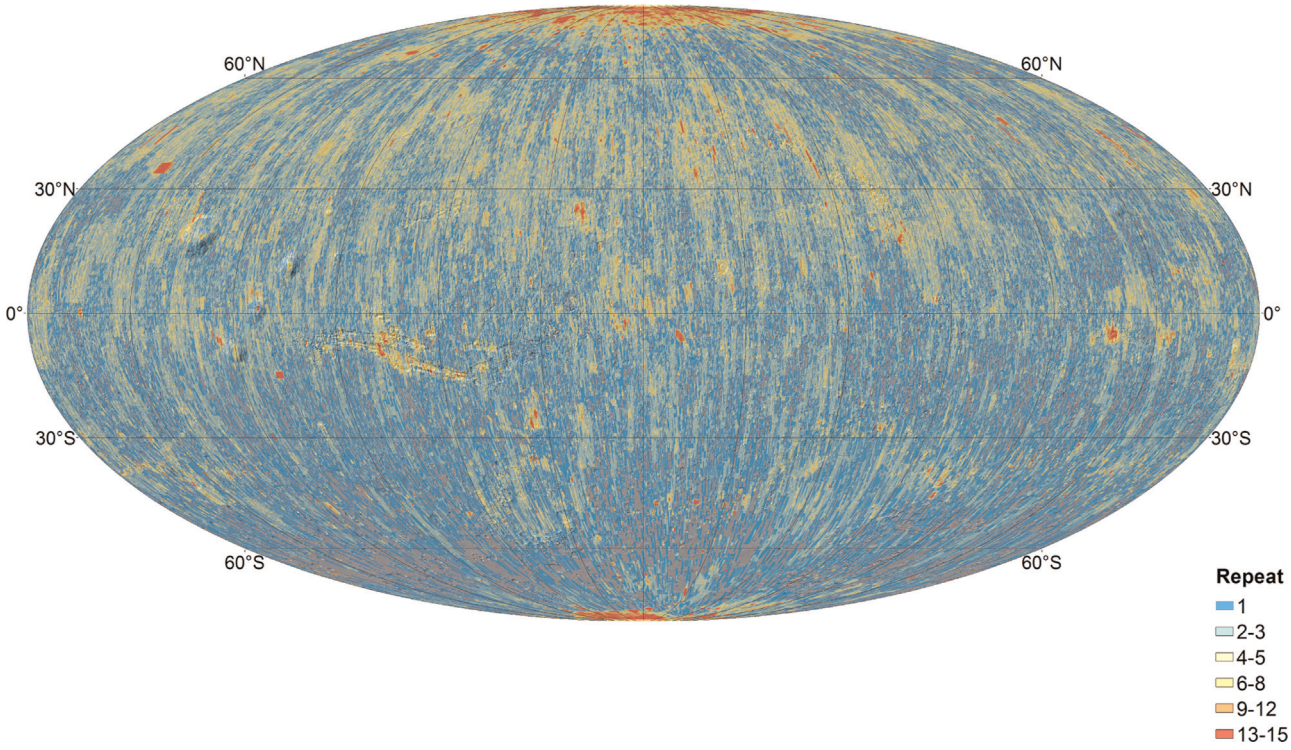


**Fig. 13.** The overall coverage of Mars with resolution finer than 20 m between Martian Years 29 and 31.

**Table 7**
An analysis of the repeat coverage spread of the high-resolution orbital images acquired on Mars.

| Class | A | B | C | D | E | F | G | H | I |
|---|---|---|---|---|---|---|---|---|---|
| Times mapped | 0 | 1 | >1 | 2 | >2 | 3 | >3 | 4 | >4 |
| Epochs mapped | 0 | 1 | 1 | 2 | 2 | 3 | 3 | 4 | 4 |
| *Res* < 20 | 3.74% | 13.25% | 28.03% | 7.72% | 43.93% | 0.16% | 3.15% | 0 | 0.01% |
| *Res* < 100 | 0.67% | 6.86% | 16.97% | 7.26% | 48.92% | 0.97% | 17.99% | 0.01% | 0.34% |

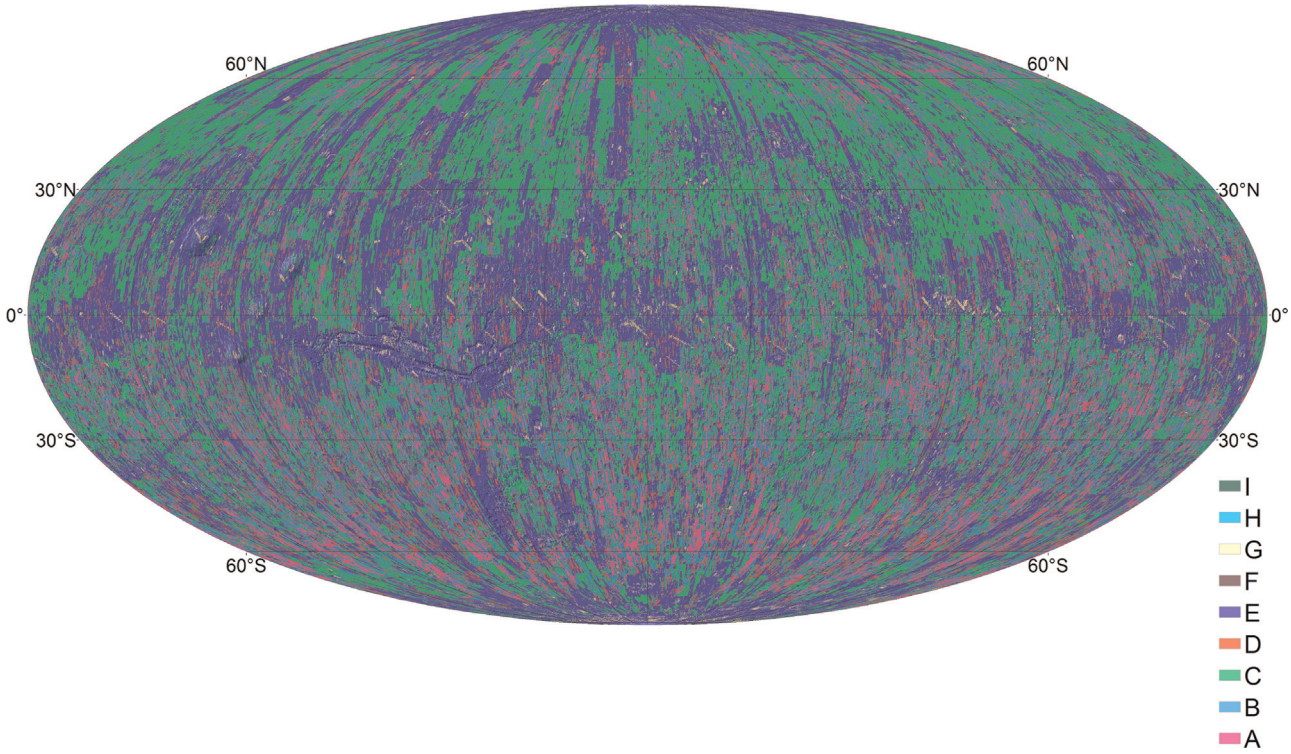


**Fig. 14.** The multi-epoch coverage of Mars.

resolution products is limited to the range 0–90°. Furthermore, it is understood that image shadows are fully determined by the incidence angle. Typically, imaging with very small or very large incidence angle is avoided, the former so as to allow shading effects (which can be used to extract 3-dimensional information through shape-from-shading techniques) and the latter because long shadows have detrimental effects in several processing stages (e.g. in stereo).

Having said that, each mission follows a distinct strategy regarding the imaging incidence angle. The Viking Orbiter team considered 70° to be ideal for imaging (Snyder, 1977), however, since Viking Orbiter was in an elliptical orbit, imaging sequences were taking place near the periapsis. Periapsis changed with time, thus drifting the incidence angle as low as 0°. Nevertheless, more than 3/5 of Viking Orbiter imaging products were acquired with an incidence angle of 61–80°. On the other hand, Mars Global Surveyor passed from the equator at 14:00, thus acquiring images near the equator with incidence angle approximately equal to 30°, while higher latitudes were acquired with larger incidence angle (Malin and Edgett, 2001).

Looking at the currently operating instruments, THEMIS-VIS acquires images between 15:00 and 16:30 local time, i.e. with an incidence angle that is typically between 45° and 75° (Kirk et al., 2005). The actual incidence angle depends on the season and the latitude. This is the case for the two cameras on-board Mars Reconnaissance Orbiter, which systematically acquire images at 15:00 local time (McEwen et al., 2007), the incidence angle varying slightly with latitude and orbital drift. The mean incidence angle of HiRISE and CTX is approximately 56°. On the contrary, HRSC is not in a sun-synchronous circular orbit but in a elliptical orbit, which along with the instrument's pointing capabilities enable imaging at all times of day (ESA, 2009). As a result, the solar elevation angles of HRSC images vary from 15° to 90°.

Fig. 15 demonstrates the incidence angle histogram of each instrument (any images of resolution coarser than 100 m are ignored). Moreover, in Table 9 the repeat coverage of Mars if grouping the high-resolution images according to the incidence angle $\theta$ is demonstrated. Table 9 demonstrates that for a large range of incidence angles the surface coverage is sparse. Actually, for $\theta < 30°$ there is no systematic repeat coverage, while for $30° < \theta < 45°$ and $75° < \theta < 90°$ the repeat coverage is limited, since for both ranges more than 70% of the martian surface has been mapped at most once. Apparently, most parts of Mars have been mapped either early in the morning or late in the afternoon, causing a homogeneity in illumination conditions that favours change detection. However, our knowledge of Mars phenomena is limited, thus the side-effects of imaging only in a limited incidence angle range are not well understood.

## 6. Products

Based on the analysis of Section 5.2 we have produced the following coverage maps of Mars:

- 3 global maps showing the overall coverage as discussed in Section 5.2 (maps “All”, “FAll” and “CAll” for resolution range 0–10 m/pixel, 0–20 m/pixel and 20–100 m/pixel, respectively).
- 8 maps showing the coverage during different epochs as discussed in Section 5.7, 4 showing the coverage with resolution

**Table 8**
An analysis of the repeat coverage spread of the high-resolution orbital images acquired on Mars.

| Res. | <1MY (%) | 1–2MY (%) | 2–3MY (%) | 3–5MY (%) | 5–10MY (%) | >10MY(%) | TMATF |
|---|---|---|---|---|---|---|---|
| 1 | 72.69 | 15.28 | 10.18 | 1.85 | 0 | 0 | $2.21 \times 10^6$ |
| 3 | 57.16 | 16.45 | 12.86 | 10.13 | 3.38 | 0 | $5.72 \times 10^6$ |
| 5 | 47.74 | 17.02 | 14.86 | 15.02 | 5.36 | 0 | $9.83 \times 10^6$ |
| 7 | 42.99 | 20.19 | 22.63 | 10.56 | 3.55 | 0 | $3.14 \times 10^8$ |
| 10 | 42.55 | 20.04 | 22.71 | 10.85 | 3.73 | 0.12 | $3.22 \times 10^8$ |
| 15 | 32.97 | 23.91 | 24.18 | 14.19 | 4.48 | 0.27 | $5.14 \times 10^8$ |
| 20 | 18.78 | 25.13 | 27.08 | 24.45 | 4.1 | 0.46 | $9.33 \times 10^8$ |
| 30 | 15.45 | 24.17 | 27.26 | 27.46 | 3.82 | 1.84 | $1.124 \times 10^9$ |
| 50 | 8.44 | 16.7 | 26.29 | 36.6 | 4.18 | 7.79 | $1.748 \times 10^9$ |
| 100 | 5.31 | 11.76 | 19.23 | 29.83 | 3 | 30.87 | $3.249 \times 10^9$ |

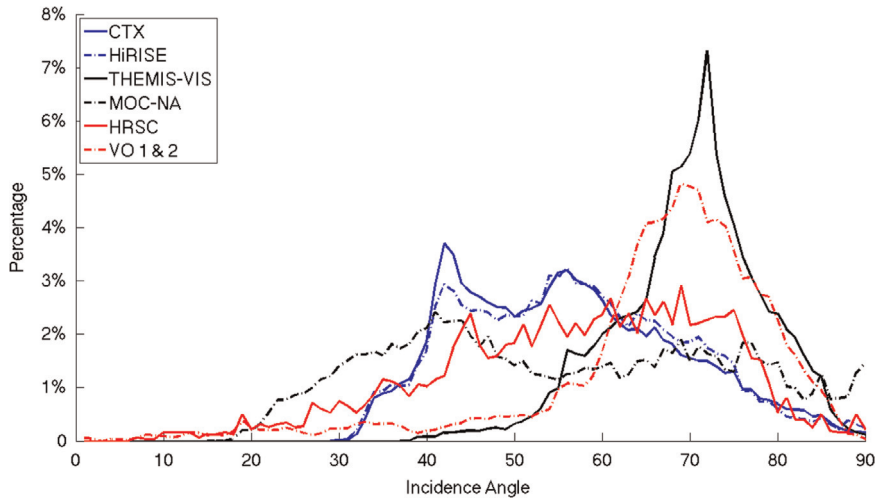


**Fig. 15.** The incidence angle histogram for each camera.

**Table 9**
The Mars surface repeat coverage that is estimated if high-resolution imaging products are grouped according to their incidence angle $\theta$.

| Repeat | $0° < \theta < 15°$ (%) | $15° < \theta < 30°$ (%) | $30° < \theta < 45°$ (%) | $45° < \theta < 60°$ (%) | $60° < \theta < 75°$ (%) | $75° < \theta < 90°$ (%) |
|---|---|---|---|---|---|---|
| 0 | 98.24 | 89.11 | 48.11 | 28.49 | 14.75 | 40.93 |
| 1 | 1.54 | 9.25 | 31.84 | 33.96 | 27.66 | 32.51 |
| 2 | 0.15 | 1.29 | 13.68 | 20.24 | 24.62 | 15.1 |
| 3 | 0.02 | 0.23 | 4.24 | 9.37 | 15 | 5.99 |
| 4 | 0.02 | 0.06 | 1.27 | 4.07 | 7.83 | 2.46 |
| >4 | 0.03 | 0.06 | 0.86 | 3.86 | 10.15 | 3.01 |

finer than 20 m (maps EpochF12, EpochF23, EpochF26 and EpochF29) and 4 showing the coverage with resolution between 20 m and 100 m (maps EpochC12, EpochC23, EpochC26 and EpochC29).
- 2 maps showing the spread coverage when taking into account images of resolution finer than 20 m/pixel and 100 m/pixel, respectively (maps MultiEpoch20 and MultiEpoch100).
- 8 maps showing the coverage during different seasons as discussed in Section 5.6, 4 showing the coverage with resolution finer than 20 m (maps SeasonF1, SeasonF2, SeasonF3 and SeasonF4) and 4 showing the coverage with resolution between 20 m and 100 m (maps SeasonC1, SeasonC2, SeasonC3 and SeasonC4).
- 8 maps showing the North and South pole coverage at different seasons for images with resolution finer than 20 m/pixel (maps SouthSpring, SouthSummer, SouthAutumn, SouthWinter, NorthSpring, NorthSummer, NorthAutumn and NorthWinter).
- 6 maps showing the coverage with different incidence angles and resolution finer than 100 m/pixel, as discussed in Section 5.8 (maps IncAng15, IncAng30, IncAng45, IncAng60, IncAng75 and IncAng90).

As already stated, the 8 polar maps use polar stereographic projection while the other 25 maps Mollweide projection. Moreover, in each map, "golden" areas depict regions that are repeatedly imaged while "bluish" areas regions that are sparsely imaged. For colouring reasons, repeat values are truncated to 20, i.e. all regions that are mapped at least 20 times are drawn with the same (red) colour. The background, which is a Mars Orbiter Laser Altimeter (MOLA) (Zuber et al., 1992) hillshaded global map of Mars, can be seen only where the repeat value is 0 (i.e. in Mars areas that were never mapped at a time and with resolution that fit on the corresponding ranges).

7 Mollweide and 2 polar stereographic maps can be found in the main body of this work ("All", "FAll", "CAll", EpochF29, MultiEpoch20, SeasonF1, SeasonF3, SouthSpring and NorthSpring). The rest are available in the supplementary materials section. The full set of coverage maps can also be found on the EU i-Mars project website.[6] Since the colour look-up table used includes red and green, we suggest that for the colourblind they use a product such as the EnChroma lens.[7]

## 7. Conclusions and future work

In this paper, we have presented a method to aggregate images according to their metadata and used this to conduct an analysis of the martian surface coverage with high-resolution imaging products. Through this analysis we have demonstrated that for a substantial part of Mars, multi-instrument pairs can be established, additionally satisfying (at least partially) constraints about the martian year and the martian season they were acquired in as well as their illumination conditions. On the other hand, the available data present two major shortcomings, the sparse stereo coverage and the narrow range of local times that most images were acquired in. The first problem is expected to be slightly attenuated in the near future with the ESA's Trace Gas Orbiter, which will be launched in 2016, having on-board the CaSSIS stereo camera (Thomas et al., 2014), with nominal goal to achieve along-track stereo coverage of 1.7% of Mars with resolution 5–10 m/pixel over 1 Martian Year. The second one would require relaxing the constraints for sun-synchronous orbiters in future imaging missions, as well as the improvement of the available modelling of the illumination conditions, which will allow the discrimination between actual surface changes and luminance variations due to different incidence angle.

Most of the results that are reported here are demonstrated in a series of global coverage maps. At the time of publication, these maps will be placed into a Web GIS which will be available from the i-Mars.eu project website. However, our main goal is to use this information, along with the martian geological context, to assess the potential of multi-instrument surface change detection for each geographic region on the martian surface. Finally, a similar analysis is also planned for the Moon in the future.

[6] www.i-mars.eu/
[7] http://enchroma.com/

## Acknowledgements

This work has received funding from the STFC MSSL Consolidated Grant ST/K000977/1 and partial support from the European Union's Seventh Framework Programme (FP7/2007-2013) under i-Mars grant agreement no 607379. We thank the anonymous referees for their helpful and informative comments which greatly enhanced the quality of the paper.

## Appendix A. Supplementary data

Supplementary data associated with this article can be found in the online version at http://dx.doi.org/10.1016/j.pss.2015.06.017.

## References

⟨http://ode.rsl.wustl.edu/mars/indextools.aspx?displaypage=footprint⟩.
Aharonson, O., Schorghofer, N., Gerstell, M.F., 2003. Slope streak formation and dust deposition rates on Mars. J. Geophys. Res.: Planets 108 (E12), 5138.
Albee, A.L., Arvidson, R.E., Palluconi, F., Thorpe, T., 2001. Overview of the Mars global surveyor mission. J. Geophys. Res. 106 (E10), 23291–23316.
Allison, M., 2008. Technical Notes on Mars Solar Time. ⟨http://www.giss.nasa.gov/tools/mars24/help/notes.html⟩.
Bell III, J.F., Malin, M.C., Caplinger, M.A., Fahle, J., Wolff, M.J., Cantor, B.A., James, P.B., Ghaemi, T., Posiolova, L.V., Ravine, M.A., Supulver, K.D., Calvin, W.M., Clancy, R.T., Edgett, K.S., Edwards, L.J., Haberle, R.M., Hale, A., Lee, S.W., Rice, M.S., Thomas, P.C., Williams, R.M.E., 2013. Calibration and performance of the Mars Reconnaissance Orbiter Context Camera (CTX). Mars 8, 1–14.
Bridges, N., Geissler, P., Silvestro, S., Banks, M., 2013. Bedform migration on Mars: current results and future plans. Aeolian Res. 9, 133–151.

Chaikin, A.L., Maxwell, T.A., El-Baz, F., 1981. Temporal changes in the Cerberus region of Mars: Mariner 9 and Viking comparisons. Icarus 45 (1), 167–178.
Christensen, P.R., Jakosky, B.M., Kieffer, H.H., Malin, M.C., McSween Jr, H.Y., Nealson, K., Mehall, G.L., Silverman, S.H., Ferry, S., Caplinger, M., Ravine, M., 2004. The Thermal Emission Imaging System (THEMIS) for the Mars 2001 Odyssey mission. Space Sci. Rev. 110 (1), 85–130.
Chuang, F.C., Beyer, R.A., Bridges, Nathan T., 2010. Modification of martian slope streaks by eolian processes. Icarus 205 (1), 154–164.
Clancy, R.T., Sandor, B.J., Wolff, M.J., Christensen, P.R., Smith, M.D., Pearl, J.C., Conrath, B.J., Wilson, R.J., 2000. An intercomparison of ground-based millimeter, MGS TES, and Viking atmospheric temperature measurements: seasonal and interannual variability of temperatures and dust loading in the global Mars atmosphere. J. Geophys. Res.: Planets 105 (E4), 9553–9571.
Cutts, J.A., Blasius, K.R., Roberts, W.J., 1979. Evolution of martian polar landscapes: interplay of long-term variations in perennial ice cover and dust storm intensity. J. Geophys. Res.: Solid Earth 84 (B6), 2975–2994.
Daubar, I.J., McEwen, A.S., Byrne, S., Kennedy, M.R., Ivanov, B., 2013. The current martian cratering rate. Icarus 225 (1), 506–516.
Dundas, C.M., Byrne, S., McEwen, A.S., Mellon, M.T., Kennedy, M.R., Daubar, I.J., Saper, L., 2014. HiRISE observations of new impact craters exposing martian ground ice. J. Geophys. Res.: Planets 119 (1), 109–127.
Dundas, C.M., Diniega, S., McEwen, A.S., 2015. Long-term monitoring of martian gully formation and evolution with MRO/HiRISE. Icarus 251 (1), 244–263.
ESA, 2009. SP-1291, Mars Express, the scientific investigations. European Space Agency.
Fenton, L.K., Geissler, P.E., Haberle, R.M., 2007. Global warming and climate forcing by recent albedo changes on Mars. Nature 446, 646–649.
Geissler, P.E., 2005. Three decades of martian surface changes. J. Geophys. Res.: Planets 110 (2), 1–23.
Gwinner, K., Scholten, F., Spiegel, M., Schmidt, R., Giese, B., Oberst, J., Heipke, C., Jaumann, R., Neukum, Gerhard, 2009. Derivation and validation of high-resolution Digital Terrain Models from Mars Express HRSC data. Photogramm. Eng. Remote Sens. 75 (9), 1127–1142.
Hansen, C.J., Diniega, S., Bridges, N., Byrne, S., Dundas, C., McEwen, A., Portyankina, G., 2015. Agents of change on Mars' northern dunes: CO2 ice and wind. Icarus 251 (1), 264–274.
Henrich, D., 1994. Space-efficient region filling in raster graphics. Vis. Comput. 10 (4), 205–215.
Hoffmann, H., the HRSC Experiment Team, 2014. HRSC/Mars Express Instrument Status and Operations. Technical Report, DLR Berlin.
Jaumann, R., Neukum, G., Behnke, T., Duxbury, T.C., Eichentopf, K., Flohrer, J., Gasselt, S.v., Giese, B., Gwinner, K., Hauber, E., Hoffmann, H., Hoffmeister, A., Köhler, U., Matz, K.-D., McCord, T.B., Mertens, V., Oberst, J., Pischel, R., Reiss, D., Ress, E., Roatsch, T., Saiger, P., Scholten, F., Schwarz, G., Stephan, K., Wählisch, M., 2007. The high-resolution stereo camera (HRSC) experiment on Mars Express: instrument aspects and experiment conduct from interplanetary cruise through the nominal mission. Planet. Space Sci. 55 (7–8), 928–952.
Kirk, R.L., Howington-Kraus, E., Archinal, B., 2002. Topographic analysis of candidate Mars Exploration Rover landing sites from MOC Narrow-Angle stereo-images. Lunar and Planetary Science Conference XXXIII.
Kirk, R.L., Soderblom, L.A., Cushing, G., Tituus, T.A., 2005. Joint analysis of visible and infrared images: a “magic airbrush” for qualitative and quantitative topography. Photogramm. Eng. Remote Sens. 71 (10), 1167–1178.
Malin, M.C., Bell, J.F., Cantor, B.A., Caplinger, M.A., Calvin, W.M., Clancy, R.T., Edgett, K.S., Edwards, L., Haberle, R.M., James, P.B., Lee, S.W., Ravine, M.A., Thomas, P.C., Wolff, M.J., 2007. Context Camera investigation on board the Mars Reconnaissance Orbiter. J. Geophys. Res.: Planets 112 (E5).
Malin, M.C., Edgett, K.S., 2001. Mars Global Surveyor Mars Orbiter Camera: interplanetary cruise through primary mission. J. Geophys. Res.: Planets 106 (E10), 23429–23570.
Malin, M.C., Edgett, K.S., Cantor, Caplinger, M.A., Danielson, E., Jensen, E.H., Ravine, M.A., Sandoval, J.L., Supulver, K.D., 2010. An overview of the 1985–2006 Mars Orbiter Camera science investigation. Mars 5, 1–60.
Malin, M.C., Edgett, K.S., Posiolova, L.V., McColley, S.M., Dobrea, E.Z.N., 2006. Present-day impact cratering rate and contemporary gully activity on Mars. Science 314 (5805), 1573–1577.
McEwen, A., Eliason, E., Bergstrom, J., Bridges, N., Hansen, C., Delamere, W., Grant, J., Gulick, V., Herkenhoff, K., Keszthelyi, L., Kirk, R., Mellon, M., Squyres, S., Thomas, N., Weitz, C., 2007. Mars Reconnaissance Orbiter's High Resolution Imaging Science Experiment (HiRISE). J. Geophys. Res.: Planets 112 (5).
McEwen, A., Ojha, L., Dundas, C., Mattson, S., Byrne, S., Wray, J., Cull, S., Murchie, S., Thomas, N., Gulick, V., 2011. Seasonal flows on warm martian slopes. Science 333 (6043), 740–743.
McEwen, A.S., Dundas, C.M., Mattson, S.S., Toigo, A.D., Ojha, L., Wray, J.J., Chojnacki, M., Byrne, S., Murchie, S.L., Thomas, N., 2014. Recurring slope lineae in equatorial regions of Mars. Nat. Geosci. 7, 53–58.
Murchie, S., Arvidson, R., Bedini, P., Beisser, K., Bibring, J.-P., Bishop, J., Boldt, J., Cavender, P., Choo, T., Clancy, R.T., Darlington, E.H., Des Marais, D., Espiritu, R., Fort, D., Green, R., Guinness, E., Hayes, J., Hash, C., Heffernan, K., Hemmler, J., Heyler, G., Humm, D., Hutcheson, J., Izenberg, N., Lee, R., Lees, J., Lohr, D., Malaret, E., Martin, T., McGovern, J.A., McGuire, P., Morris, R., Mgustard, J., Pelkey, S., Rhodes, E., Robinson, M., Roush, T., Schaefer, E., Seagrave, G., Seelos, F., Silverglate, P., Slavney, S., Smith, M., Shyong, W.-J., Strohbehn, K., Taylor, H., Thompson, P., Tossman, B., Wirzburger, M., Wolff, M., 2007. Compact Reconnaissance Imaging Spectrometer for Mars (CRISM) on Mars Reconnaissance Orbiter (MRO). J. Geophys. Res.: Planets 112 (E5).
Neukum, G., Jaumann, R., HRSC Co-Investigator Team, 2004. Mars Express: The Scientific Payload, chapter HRSC: The High Resolution Stereo Camera of Mars Express. European Space Agency, Netherlands.
NASA Scientific & Technical Information Office, 1974. SP-329, Mars as viewed from Mariner 9. U.S. National Aeronautics and Space Administration.
Piqueux, S., Byrne, S., Richardson, M.I., 2003. Sublimation of Mars's southern seasonal CO2 ice cap and the formation of spiders. J. Geophys. Res.: Planets 108 (E8), 1–9.
Scholten, F., Gwinner, K., Roatsch, T., Matz, K.D., Wählisch, M., Giese, B., Oberst, J., Jaumann, R., Neukum, G., 2005. and the HRSC Co-Investigator Team, 2005. Mars Express HRSC data processing-methods and operational aspects. Photogramm. Eng. Remote Sens. 71, 1143–1152.
Schorghofer, N., Aharonson, O., Gerstell, M.F., Tatsumi, L., 2007. Three decades of slope streak activity on Mars. Icarus 192 (1), 132–140.
Schorghofer, N., King, C.M., 2011. Sporadic formation of slope streaks on Mars. Icarus 216 (1), 159–168.
Smith, M.D., 2009. THEMIS observations of Mars aerosol optical depth from 2002–2008. Icarus 202 (2), 444–452.
Snyder, C.W., 1977. The missions of the Viking Orbiters. J. Geophys. Res. 82 (28), 3971–3983.
Snyder, J.P., 1987. Map Projections: A Working Manual. U.S. Geological Survey.
Soffen, G.A., 1976. Scientific results of the Viking mission. Science 194 (4271), 1274–1276.
Soffen, G.A., Snyder, C.W., 1976. The first Viking mission to Mars. Science 193 (4255), 759–766.
Thomas, N., Cremonese, G., Banaszkiewicz, M., Bridges, J., Byrne, S., Deppo, V.D., et al., 2014. The colour and stereo surface imaging system (CaSSIS) for ESA's Trace Gas Orbiter. In: 8th International Conference on Mars.
Thomas, N., Hansen, C.J., Portyankina, G., Russell, P.S., 2010. HiRISE observations of gas sublimation-driven activity in Mars southern polar regions: Ii. surficial deposits and their origins. Nat. Geosci. 205 (1), 296–310.
Thornhill, G.D., Rothery, D.A., Murray, J.B., Cook, A.C., Day, T., Muller, J.P., Iliffe, J.C., 1993. Topography of Apollinaris-Patera and Maadim-Vallis—automated extraction of digital elevation models. J. Geophys. Res.: Planets 98 (E12), 23581–23587.
van Gasselt, S. (FUB), Gwinner K. (DLR), 2015. Private communication.
Verba, C.A., Geissler, P.E., Titus, T.N., Waller, D., 2010. Observations from the High Resolution Imaging Science Experiment (HiRISE): Martian dust devils in Gusev and Russell craters. J. Geophys. Res.: Planets 115 (E9), 1–11.
Zuber, M.T., Smith, D.E., Solomon, S.C., Muhleman, D.O., Head, J.W., Garvin, J.B., Abshire, J.B., Bufton, J.L., 1992. The Mars Observer laser altimeter investigation. J. Geophys. Res. 97 (E5), 7781–7797.
Zurek, R.W., Smrekar, S.E., 2007. An overview of the Mars Reconnaissance Orbiter (MRO) science mission. J. Geophys. Res. E05 (S01).